This is to certify that the
dissertation entitled

COMPUTATIONALLY EFFICIENT CRYSTAL PLASTICITY
MODELS FOR POLYCRYSTALLINE MATERIALS

presented by

Amir Reza Zamiri

has been accepted towards fulfillment
of the requirements for the

___PhD___   degree in   ___Mechanical Engineering___

_____
Major Professor's Signature

_____11/05/2008_____

Date

PLACE IN RETURN BOX to remove this checkout from your record.
TO AVOID FINES return on or before date due.
MAY BE RECALLED with earlier due date if requested.

DATE DUE	DATE DUE	DATE DUE

COMPUTATIONALLY EFFICIENT CRYSTAL PLASTICITY
MODELS FOR POLYCRYSTALLINE MATERIALS

By

Amir Reza Zamiri

A DISSERTATION

Submitted to
Michigan State University
in partial fulfillment of the requirements
for the degree of

DOCTOR OF PHILOSOPHY

Mechanical Engineering

2008

ABSTRACT

COMPUTATIONALLY EFFICIENT CRYSTAL PLASTICITY MODELS FOR POLYCRYSTALLINE MATERIALS

By

Amir Reza Zamiri

Crystal plasticity models have been successfully used to take into account the effect of microstructure in modeling and designing crystalline materials. Up to now, several computational methods for crystal plasticity models have been proposed. The main objectives of these computational methods have been to overcome the problem arising from the non-uniqueness of active slip systems during the plastic deformation of a crystal and to increase the efficiency and computational speed. The problem with most current models is that either they are not efficient for all strain paths or are very expensive. In this thesis, three new computational methods are developed for crystal plasticity which are believed to be the most efficient and the fastest crystal plasticity models currently available. In the first model, the current single crystal yield function is modified to decrease the degree of nonlinearity of the model and increase its computational speed. The second model, which is a temperature and microstructure sensitive, is a bridge between computational mechanics and dislocation theory. The results of this model have been very impressive. The third model, the so called combined constraints model, is based on developing a new yield function for a single crystal to overcome the problem arising from the current proposed highly nonlinear yield functions for a single crystal. These models were implemented into

ABAQUS/Explicit finite element code and two cases of uniaxial tension and tube hydroforming were simulated using these models. Finally, the combined constraints model was used to investigate the plasticity induced surface roughness in polycrystalline high purity niobium. The results of the newly proposed single crystal model showed a good match with experimental data. Also, compared with other crystal plasticity models such as the singular value decomposition multi-yield surface crystal plasticity model and Gambin model, the proposed crystal plasticity models were more efficient and computationally faster.

ACKNOWLEDGMENTS

TABLE OF CONTENTS

LIST OF TABLES

LIST OF FIGURES

Images in this thesis/dissertation are presented in color

CHAPTER 1

INTRODUCTION

Crystal plasticity has recently attracted many attentions due to its ability to relate the plastic behavior of the crystalline materials to their microstructures. Crystal plasticity can be successfully used in modeling such phenomena as; microcrack initiation, crack propagation, fatigue, creep in small scale plasticity, texture design, calculation of damage parameters, evolutionary coefficients of yield functions, fracture criteria and FLD diagram, etc in crystalline materials. The fundamental importance of single crystal modeling is reflected by the abundance of theories on monocrystalline plasticity in the literature. Such theories began to appear in the literature in the early 20th century and are presented by many investigators, including: Taylor, Schmid, Hill, Rice, Hutchinson, Asaro, Havner, Bassani, Mandel and Kocks. Taylor first showed that five independent slip systems are needed to accommodate an arbitrary strain increment imposed on a crystal (Taylor, 1938). The Schmid law states that in response to applied loads on a single crystal, slip occurs when the resolved shear stress on a crystallographic slip system (uniquely defined by a slip direction and a slip plane normal) exceeds a critical value that is a material property (Schmid and Boas, 1935). The continuum mechanics framework provided the necessary foundations to develop a systematic computational methodology for performing the first detailed numerical simulations of single crystals including their localization behavior (Peirce et al., 1982). Early simulations were 2D plane strain based on the Asaro's (1979) planar double slip model and provided insights into nonuniform and localized

deformation in single crystals. They were further extended to include modeling of polycrystals and other problems of interest. Due to an increase in computational resources that became available, full-scale three dimensional simulations of crystalline solids undergoing multislip (fcc, bcc) became increasingly feasible (e.g., Cuitino and Ortiz, 1992; Kalidindi et al., 1992). However, the complexity of the structure of governing equations and large number of internal variables in crystal plasticity models generally makes the 3D numerical simulations intensive and time consuming.

In order to describe the plastic deformation by the crystallographic glide, three successive steps must be accomplished; determination of the active slip systems, determination of the increments of shear on the active slip systems, and overcoming the problem arising from non-uniqueness of active slip systems due to interdependency of the slip systems in an arbitrary strain path. Several algorithms have been proposed to overcome the numerical problems due to interdependency of slip systems in plastic deformation of crystalline materials. One approach has been rate-dependent formulations without an elastic domain based on power-type creep laws without differentiation of slip systems into active and inactive sets, see Pierce et al. (1982, 1983), Asaro and Needleman (1985), Mathur and Dawson (1989) and Huang (1991). Some investigations show that algorithms based on multisurface yield functions can be the most effective techniques in crystal plasticity, however, in the rate-independent model under a particular mode of hardening, the constraints of the multisurface framework are redundant. Cuitino and Ortiz (1992) used a multisurface viscoplastic model with elastic domain to overcome this problem. Anand and Kothari

(1996) overcame this redundancy by using the singular value decomposition technique in the inversion of the Jacobian of the active slip systems. Miehe and Schroder (1999, 2001) suggested two methods of alternative general inverse where a reduced space is obtained by dropping columns of the local Jacobian associated with zero diagonal elements within a standard factorization procedure and diagonal shift of the Jacobian of the active yield criterion functions to overcome this problem. However, these procedures are very expensive and deficient at times. Raphanel et al. (2004) proposed a crystal plasticity model based on Runge-Kutta algorithms. McGinty and McDowell (2006) introduced a semi-implicit integration scheme for rate independent crystal plasticity. Nemat-Nasser et al. (1996), Knoekaert et al. (2000), and McGinty and McDowell (2006) used a formulation based on the consistency condition during plastic flow to improve the speed and stability relative to the multiplicative decomposition formulation. The behavior, accuracy, and the efficiency of some of the above crystal plasticity models have been examined by several investigators; Busso and Cailletaud (2005), for example, evaluated the set of active slip systems predicted by several models. Ling et al. (2005) compared the stress–strain response and the speed of several models using several explicit and implicit formulations. They also examined the overall running times for single-crystal updates. Rousselier and Leclercq (2006) compare the overall running times of several polycrystal models. Kuchnicki et al. (2006) investigated the efficiency of the Cuitino and Ortiz (1993) model both in implicit and explicit update procedures.

Montheillet et al. (1985), Van Houtte (1987), Lequeu (1987), Toth et al. (1991), Arminjon (1991), Darrieulat and Piot (1996), and Gambin (1991, 1992, 1997)

proposed a rate-independent approach based on the concept of crystals with smooth yield surfaces. In this formulation only one yield function is considered to calculate the crystal spin and incremental shear strains on active slip systems. Therefore, the slip system ambiguity problem in crystal plasticity is avoided. Gambin correlated the degree of the non-linearity of the yield function (i.e., its exponential power) to the stacking fault energy (SFE) of the material. In this model, the shape of a single crystal's yield surface, i.e. with sharp or rounded corners, can be correlated with high and low SFE, respectively. Based on this formulation, for a material with high SFE, such as aluminum, a highly nonlinear yield function should be used in order to reasonably predict the texture of the material after deformation. This, however, makes the computation to be very expensive. Using a lower degree of non-linearity for the yield function (i.e., lower exponential power) produces incompatibility in different grain spins in polycrystalline materials, which leads to an oscillation in the calculated stresses.

The objective of this work is to find easier and more efficient approaches to solve a crystal plasticity problem. Three distinct approaches have been followed in order to develop effective numerical methods to address crystal plasticity problems. In the first method, the current yield function for a single crystal is modified such that the experimental data is captured accurately while increasing the computational speed. In the second method, physical models expressing the relationship between the resolved shear stress and dislocation velocity, the so called dislocation dynamics models, are used to solve the crystal plasticity problem. Finally, in the third method a new yield function is introduced in order to model the crystal deformation.

4

The fundamentals of crystal plasticity and governing equations are briefly introduced in chapter 2. The mathematical details of the three methods are discussed in chapters 3, 4, and 5. In chapter 6, a solution algorithm for the proposed models will be presented. The evaluation of the proposed crystal plasticity models will be discussed in chapter 7, in which some preliminary examples of simulating the plastic deformation of a fcc polycrystal subjected to uniaxial tension and tube hydroforming will be presented. In chapter 8, the combined constraints crystal plasticity model are used to model the plasticity induced surface roughness in high purity superconducting niobium as an example of application of the models for bcc materials.

CHAPTER 2

FRAMWORK FOR CRYSTAL PLASTICITY

2.1. Basic Kinematics and Constitutive Equations

Two different coordinate systems will be considered; the material co-rotational (i.e., attached to a finite element) and the crystal coordinate system (i.e., defining the crystal axes of a single crystal). A general formulation can be developed using the material co-rotational system. Let **m** be a unit vector normal to the slip plane and **s** a unit vector in the slip direction in the crystal coordinate system. Then, any slip system at the beginning of the strain increment can be defined by the matrix $\mathbf{I}_0^{\alpha}$ as:

$$\mathbf{I}_0^{\alpha} = \mathbf{m}^{\alpha} \otimes \mathbf{s}^{\alpha} \tag{2.1}$$

The deformation in a single crystal can be decomposed into two parts; the elastic deformation, which is responsible for the lattice rotation, and the plastic deformation, which is caused solely by crystalline slip. Therefore, the total velocity gradient in current state can be expressed as:

$$\mathbf{L} = \mathbf{L}^* + \mathbf{L}^p = \mathbf{D} + \mathbf{\Omega} \tag{2.2}$$

where the symmetric rate of deformation **D** and the antisymmetric spin tensor **Ω** may be decomposed into elastic and plastic part as follows:

$$\mathbf{D} = \mathbf{D}^* + \mathbf{D}^P \tag{2.3}$$

$$\mathbf{\Omega} = \mathbf{\Omega}^* + \mathbf{\Omega}^P \tag{2.4}$$

6

The lattice spin rate $\mathbf{\Omega}^*$ is defined by:

$$\mathbf{\Omega}^* = \dot{\mathbf{R}}^* \mathbf{R}^{*T}$$

(2.5)

where $\mathbf{R}^*$ is the rigid body rotation of the lattice.

Now with respect to the material co-rotational coordinate system:

$$\mathbf{I}^\alpha = \mathbf{R}^* \mathbf{I}_0^\alpha \mathbf{R}^{*T}$$

(2.6)

The symmetric and antisymmetric parts of the slip system are then expressed by $\mathbf{P}^\alpha$

and $\mathbf{W}^\alpha$, where:

$$\mathbf{P}^\alpha = \frac{1}{2}\left(\mathbf{I}^\alpha + \mathbf{I}^{\alpha T} \right)$$

(2.6)

$$\mathbf{w}^\alpha = \frac{1}{2}\left(\mathbf{I}^\alpha - \mathbf{I}^{\alpha T} \right)$$

(2.7)

The plastic rate of deformation $\mathbf{D}^p$ and spin rate $\mathbf{\Omega}^p$ of a single crystal are (Huang Y. (1991)):

$$\mathbf{D}^p = \sum_{\alpha=1}^{N} \dot{\gamma}^\alpha \cdot \mathbf{P}^\alpha$$

(2.8)

$$\mathbf{\Omega}^p = \sum_{\alpha=1}^{N} \dot{\gamma}^\alpha \cdot \mathbf{w}^\alpha$$

(2.9)

where N is the number of slip systems, and $\dot{\gamma}^\alpha$ is shear slip rate. $\mathbf{D}^p$ corresponds to the rate of deformation of a single crystal and $\mathbf{\Omega}^p$ to the spin of a single crystal defined in the co-rotational system.

Equation (2.4) shows two different rotations during a deformation increment; one is the rotation of the material co-rotational frame, which is due to macroscopic spin $\mathbf{\Omega}$, and the other one is the rotation of the crystal coordinate system, which is due to the microscopic spin, $\mathbf{\Omega}^*$. Therefore, the macroscopic and microscopic co-rotational stress rate, $\overset{\triangledown}{\sigma}$, and $\overset{\triangledown^*}{\sigma}$ respectively are defined as:

$$\overset{\triangledown}{\sigma} = \dot{\sigma} - \Omega\sigma + \sigma\Omega \tag{2.10}$$

$$\overset{\triangledown^*}{\sigma} = \dot{\sigma} - \Omega^*\sigma + \sigma\Omega^* \tag{2.11}$$

where $\dot{\sigma}$ is the stress rate in the co-rotational coordinate system. The co-rotational stress rate on the material axes can be related to the co-rotational axes on the crystal coordinate by:

$$\overset{\triangledown}{\sigma} = \overset{\triangledown^*}{\sigma} - \left(\Omega - \Omega^*\right)\sigma + \sigma\left(\Omega - \Omega^*\right) \tag{2.12}$$

For metallic materials the elastic deformation is usually very small. Therefore, the relation between the symmetric rate of stretching of the lattice and the Jaumann rate of the Cauchy stress, $\overset{\triangledown^*}{\sigma}$, is given by:

$$\overset{\nabla^{*}}{\boldsymbol{\sigma}} = \mathbf{C}^{e} : \mathbf{D}^{*} \tag{2.13}$$

where $\mathbf{C}^{e}$ is the fourth order tensor of anisotropic elastic moduli.

2.2 Hardening

For a crystal plasticity problem one needs to know the evolution of the τ_{y}^{α} (critical shear stress of slip systems) with plastic shear. Let us consider $g^{\alpha} = \tau_{y}^{\alpha}$ as the current slip resistance on slip system α, which evolves from the critical resolved shear stress τ_{0}^{α} with plastic slip on the active slip systems. The evolution of g^{α} is expressed by the following hardening equation [Asaro and Needleman (1985)]:

$$\dot{g}^{\alpha} = \sum_{\beta=1}^{N} h^{\alpha\beta} \left| \dot{\gamma}^{\beta} \right| \tag{2.14}$$

where $\dot{\gamma}^{\beta}$ is the plastic slip rate on the active slip system β and $h^{\alpha\beta}$ are denoted as the components of the hardening matrix. The $h^{\alpha\alpha}$ are known as the self-hardening moduli while $h^{\alpha\beta}$ for ($\alpha \neq \beta$) are known as the latent-hardening moduli. The hardening matrix plays an important role in the hardening model. Several equations have been proposed for the hardening matrix. Hutchinson (1976), Chang and Asaro (1981), Bassani and Wu (1991) and Peirce et al. (1982) proposed the following simple law:

$$h^{\alpha\beta} = h^{\beta}[q + (1-q)\delta^{\alpha\beta}] \quad \text{(no summation on } \beta) \tag{2.15}$$

9

Here q is the so-called latent-hardening ratio which is the ratio of the latent-hardening rate to the self-hardening rate of a slip system with the values in the range of $1 < q$ <1.4. It can be considered 1 for coplanar slip systems and 1.4 for non-coplanar slip systems. h^β is an evolutionary function denoting the self-hardening rate, which can be expressed as a function of either shear slips or resolved shear stress on slip systems. Based on Kothari and Anand (1996), h^β was considered to evolve as:

$$h^\beta = h_0 \left| 1 - \frac{g^\beta}{\tau_s} \right|^a \cdot \mathrm{sgn}\left(1 - \frac{g^\beta}{\tau_s} \right) \tag{2.16}$$

Where h_0, a and τ_s are slip system hardening parameters, which are considered to be identical for all slip systems. h_0 denotes the initial hardening rate, τ_s the saturation value of the slip resistance, and a the exponent describing the shape of the function (equation 2.16).

2.3 Crystal Spin and Rotation

The initial orientation of a grain is given by the knowledge of the mapping from the laboratory frame to the crystallographic coordinate of the crystal. This mapping is a rotation, which defines the initial orientation matrix $\mathbf{Q}$ of the crystal. The initial orientation matrix may be constructed using Euler angles. In this case, the columns and rows of the matrix may be interpreted as the crystallographic axes in the symmetric and Bunge conventions for the Euler angles, respectively. One of the most important parts of a crystal plasticity algorithm is to correctly calculate the grain

rotation due to an imposed plastic deformation. In the material co-rotational coordinate system, the relative spin tensor is defined as:

$$\boldsymbol{\Omega} = \mathbf{W} - \dot{\mathbf{R}}\mathbf{R}^{T}$$

(2.17)

where $\mathbf{W}$ is the spin tensor, and $\boldsymbol{\Omega}$ can be decomposed into the elastic part $\boldsymbol{\Omega}^{*}$ and the plastic part $\boldsymbol{\Omega}^{p}$ as:

$$\boldsymbol{\Omega} = \boldsymbol{\Omega}^{*} + \boldsymbol{\Omega}^{p}$$

(2.18)

And in the material coordinate system:

$$\boldsymbol{\Omega} = \boldsymbol{\Omega}^{*} + \boldsymbol{\Omega}^{p} = \dot{\mathbf{R}}^{*}\mathbf{R}^{*T} + \sum_{\alpha=1}^{N} \mathbf{w}^{\alpha} \cdot \dot{\gamma}^{\alpha}$$

(2.19)

It must be mentioned that $\mathbf{w}^{\alpha}$ is in the material coordinate system.

Then the lattice spin $\boldsymbol{\Omega}^{*}$ can be obtained from equation (2.19) as:

$$\boldsymbol{\Omega}^{*} = \boldsymbol{\Omega} - \sum_{\alpha=1}^{N} \mathbf{w}^{\alpha} \cdot \dot{\gamma}^{\alpha}$$

(2.20)

The rigid body rotation matrix in an incremental form can be expressed as:

$$\begin{aligned}
\mathbf{R}_{t_0+\Delta t} &= \mathbf{R}_{t_0} + \dot{\mathbf{R}}_{t_0+\Delta t}\Delta t \\
&= [\mathbf{I} + \dot{\mathbf{R}}_{t_0+\Delta t}\mathbf{R}_{t_0}{}^{T}\Delta t]\mathbf{R}_{t_0} \\
&= [\mathbf{I} + \boldsymbol{\Omega}_{t+\Delta t}\Delta t]\mathbf{R}_{t_0}
\end{aligned}$$

(2.21)

Based on the above equation, one can easily write a similar equation for updating the grain orientation:

11

$$\begin{aligned}
\mathbf{Q}_{t_0+\Delta t} &= \mathbf{Q}_{t_0} + \Delta\mathbf{Q} \\
&= [\mathbf{I} + \boldsymbol{\Omega}^{*}\Delta t]\mathbf{Q}_{t_0} \\
&= \left[\mathbf{I} + \left(\boldsymbol{\Omega} - \sum_{\alpha=1}^{N}\mathbf{w}^{\alpha}\cdot\dot{\gamma}^{\alpha}\right)\Delta t\right]\mathbf{Q}_{t_0}
\end{aligned} \tag{2.22}$$

where $\mathbf{Q}$ is an orientation matrix defined in Appendix A.

The crystal orientation matrix updated by equation (2.22) may not have the property of the rotation tensor. Simo and Vu-Quoc (1986) suggested the following equation to update the rotation matrix:

$$\mathbf{Q}_{t_0+\Delta t} = Exp\left[\left(\boldsymbol{\Omega} - \sum_{\alpha=1}^{N}\mathbf{w}^{\alpha}\cdot\dot{\gamma}^{\alpha}\right)\Delta t\right]\mathbf{Q}_{t_0} \tag{2.23}$$

The exponential part of the above equation is an orthogonal tensor that can be determined by the Rodrigues formula as:

$$Exp(\boldsymbol{\Omega}^{*}\Delta t) = \mathbf{I} + \frac{\sin(\Omega^{e}\Delta t)}{\Omega^{e}}\boldsymbol{\Omega}^{*} + \frac{1-\cos(\Omega^{e}\Delta t)}{\left(\Omega^{e}\right)^{2}}\left(\boldsymbol{\Omega}^{*}\right)^{2} \tag{2.24}$$

with $\Omega^{e} = \sqrt{\left(\boldsymbol{\Omega}^{*}:\boldsymbol{\Omega}^{*}\right)/2}$.

However, equation (2.23) seems to introduce some stability problems in the integration algorithm especially in larger increment times.

Here a grain orientation updating procedure is used based on Pourboghrat and Barlat (2002). Consider equation (2.18), then matrix $\boldsymbol{\Omega}^{*}$ can be considered as a matrix made of three column vectors as:

12

$$\Omega^* = \begin{bmatrix} \Gamma_1 & \Gamma_2 & \Gamma_3 \end{bmatrix} \tag{2.25}$$

Then the rotation axis $\mathbf{r}$ can be defined as:

$$\mathbf{r} = \frac{\Gamma_2 \times \Gamma_3}{|\Gamma_2 \times \Gamma_3|}, \text{ or} \qquad \mathbf{r} = \frac{\Gamma_3 \times \Gamma_1}{|\Gamma_3 \times \Gamma_1|}, \text{ or} \qquad \mathbf{r} = \frac{\Gamma_1 \times \Gamma_2}{|\Gamma_1 \times \Gamma_2|}$$

The rotation angle is:

$$tg\zeta_i = \frac{\text{sgn}(\mathbf{r}.\mathbf{Q}_i \times \Delta\mathbf{Q}_i)|\Delta\mathbf{Q}_i|}{\sqrt{1-(\mathbf{r}.\mathbf{Q}_i)^2}} \tag{2.26}$$

where $\mathbf{Q}_i$'s are the column vectors in crystal orientation matrix $\mathbf{Q}$ at the beginning of

the increment and $\Delta\mathbf{Q}_i = \Omega^*\mathbf{Q}_i\Delta t$.

Now it can be shown that:

$$\mathbf{Q}_i' = \cos\zeta_i\mathbf{Q}_i + (\mathbf{r}.\mathbf{Q}_i)(1-\cos\zeta_i)\mathbf{r} + \sin\zeta_i\mathbf{r} \times \mathbf{Q}_i = $$
$$P_{i1}\mathbf{Q}_1 + P_{i2}\mathbf{Q}_2 + P_{i3}\mathbf{Q}_3 \tag{2.27}$$

Where $\mathbf{Q}_i'$s are the column vectors of $\mathbf{Q}$ after rotation at the end of the increment and

transformation matrix $\mathbf{P}$ is defined as:

$$\mathbf{P} = \begin{bmatrix} r_1^2(1-\cos\zeta_1)+\cos\zeta_1 & r_1r_2(1-\cos\zeta_2)+r_3\sin\zeta_2 & r_1r_3(1-\cos\zeta_3)-r_2\sin\zeta_3 \\ r_2r_1(1-\cos\zeta_1)-r_3\sin\zeta_1 & r_2^2(1-\cos\zeta_2)+\cos\zeta_2 & r_2r_3(1-\cos\zeta_3)+r_1\sin\zeta_3 \\ r_3r_1(1-\cos\zeta_1)+r_2\sin\zeta_1 & r_3r_2(1-\cos\zeta_2)-r_1\sin\zeta_2 & r_3^2(1-\cos\zeta_3)+\cos\zeta_3 \end{bmatrix}$$
$$\tag{2.29}$$

2.4 Homogenization

In this numerical calculation, the Taylor type homogenization model (Taylor (1983)) is used. According to the Taylor model, which is an upper bound model, each grain of the polycrystal undergoes the same deformation and deformation rate. Therefore, the velocity gradients in all grains are the same and equal to the macroscopic velocity gradient.

A velocity gradient in the material coordinate system can be decomposed into a rate of deformation and spin tensor as:

$$\mathbf{L} = \mathbf{D} + \mathbf{W} \tag{2.30}$$

Then according to Taylor's model (Chin and Mammel (1969)), the spin tensor $\mathbf{W}$ would also be the same in all grains and equal to the macroscopic $\mathbf{W}$. It must be mentioned that $\mathbf{\Omega}^*$ and $\mathbf{\Omega}^P$ would be different in different grains.

According to the theory of the grain averages in polycrystalline materials, the volume average of a local tensorial quantity $\mathbf{t}(x)$ is defined as the volume average of each tensor component and will be denoted by $\langle \mathbf{t} \rangle$:

$$\langle \mathbf{t} \rangle = \frac{1}{V} \int_V \mathbf{t}(x) dV \tag{2.31}$$

Now the average stress tensor in a polycrystalline material can be expressed as a summation of crystals c:

$$\langle \mathbf{\sigma} \rangle = \frac{1}{V} \int_V \mathbf{\sigma}^c(x) dV \tag{2.32}$$

14

Assuming that $\sigma^c(x)$'s are constant over the grain domains and grains have the same volume, equation (2.32) can be rewritten as:

$$\langle \sigma \rangle = \frac{V^c}{V} \sum_c \sigma^c = \frac{1}{M} \sum_c \sigma^c \tag{2.33}$$

Where V^c is the grain volume, σ^c the grain stress tensor, and M the number of grains.

Equation (2.33) is used in implicit and explicit algorithms to calculate the average stress tensor from the crystal stress tensors.

CHAPTER 3

MODIFIED SINGLE CRYSTAL POWER-LAW TYPE YIELD FUNCTION (MODIFIED GAMBIN'S MODEL)

3.1 Basics of Single Crystal Power-Law Type Yield Function

The idea of using a single crystal yield surface with round corners is a powerful approach in overcoming the slip system ambiguity problem in a rate-independent crystal plasticity model. In this formulation only one yield function is used in order to calculate the crystal spin and incremental shear strains on active slip systems. The idea first was introduced by Montheillet et al. (1985) and then was incrementally improved by Van Houtte (1987), Lequeu (1987), Toth et al. (1991), Arminjon (1991), Darrieulat and Piot (1996), and Gambin (1991, 1992, 1997). Based on this expression of yield function the shear strain rate on any active slip system can be expressed as:

$$\dot{\gamma}^\alpha = \lambda \frac{\mathrm{sgn}(\tau^\alpha)}{\tau_0^\alpha} \left| \frac{\tau^\alpha}{\tau_0^\alpha} \right|^{2n-1} \tag{3.1}$$

where τ^α is the resolved shear stress on the slip system which can be related to the stress tensor in the fixed coordinate system by:

$$\tau^\alpha = \hat{\sigma} : \mathbf{P}^\alpha \tag{3.2}$$

where $\hat{\sigma}$ is the rotated stress tensor back to the fixed coordinate system.

λ is a positive parameter which depends on the type of dislocation barriers and defined as:

$$\lambda = ab^{\alpha} \rho_m^{\alpha} \omega_0 \tag{3.3}$$

where a is a constant, b is the Berger's vector, ρ_m is the average dislocation density on the slip system, and ω_0 is the frequency of the passing barriers by dislocations. τ_0^{α} is the critical resolved shear stress on the active slip system.

Assuming that parameter λ is the same for all slip systems, then by substituting for shear strain rate from equation (3.1) into equations (3.2) and (3.3):

$$\mathbf{D}^p = \lambda \sum_{\alpha=1}^{N} \frac{\mathrm{sgn}(\tau^{\alpha})}{\tau_0^{\alpha}} \left| \frac{\boldsymbol{\sigma} : \mathbf{P}^{\alpha}}{\tau_0^{\alpha}} \right|^{2n-1} \cdot \mathbf{P}^{\alpha} \tag{3.4}$$

$$\boldsymbol{\Omega}^p = \lambda \sum_{\alpha=1}^{N} \frac{\mathrm{sgn}(\tau^{\alpha})}{\tau_0^{\alpha}} \left| \frac{\boldsymbol{\sigma} : \mathbf{P}^{\alpha}}{\tau_0^{\alpha}} \right|^{2n-1} \cdot \mathbf{w}^{\alpha} \tag{3.5}$$

Considering equations (3.4) and (3.5) and remembering the concept of the normality rule, one can introduce a plastic potential with respect to crystal coordinate system as:

$$\phi\left(\boldsymbol{\sigma}, \tau_c^{\alpha}, \boldsymbol{\Phi}\right) = \frac{1}{2n} \left(\sum_{\alpha=1}^{N} \left| \frac{\boldsymbol{\sigma} : \mathbf{P}^{\alpha}}{\tau_c^{\alpha}} \right|^{2n} - 1 \right) \tag{3.6}$$

where $\boldsymbol{\Phi}$ is a vector containing the three Euler angles defining the orientation of the crystal with respect to the material co-rotational coordinate system at any deformation step and it arises from the dependency of $\mathbf{P}^{\alpha}$ on Euler angles.

3.2 Modified Single Crystal Power-Law Yield Surface

In contrast to Gambin's yield function, which is defined in the fixed coordinate system, we define the above crystal yield function in the crystal coordinate system. Therefore, the plastic potential in equation (3.6) is independent of Euler angles, or in other words $\mathbf{P}^{\alpha}$ remains constant. These modifications reduce the computational time and also allow using a value for n (the degree of yield function non-linearity) that is half of that used in the Gambin's original model without losing the stability in computed stresses and grain's spin rate. Based on this formulation, a crystal orientation tensor, $\mathbf{Q}$, is defined, which defines the orientation of the crystal coordinate system with respect to the material coordinate system. Stress tensor in crystal frame, $\boldsymbol{\sigma}^{*}$, can be computed using equation (2.13) and stress tensor in material coordinate system can be obtained by the following transformation,

$$\boldsymbol{\sigma} = \mathbf{Q}^{T} \boldsymbol{\sigma}^{*} \mathbf{Q} \tag{3.7}$$

A yield function with respect to the crystal coordinate system is defined as:

$$\phi\left(\boldsymbol{\sigma}^{*}, \tau_{c}^{\alpha}\right) = \frac{1}{2n^{*}} \left(\sum_{\alpha=1}^{N} \left| \frac{\boldsymbol{\sigma}^{*} : \mathbf{P}_{0}^{\alpha}}{\tau_{c}^{\alpha}} \right|^{2n^{*}} - \zeta \right) \tag{3.8}$$

where ζ is suggested to be:

$$\zeta = \left[\frac{1}{kN} \sum_{\alpha=1}^{N} \sum_{\beta=1}^{N} \left| \mathbf{P}_{0}^{\alpha} : \mathbf{P}_{0}^{\beta} \right| \right] \tag{3.9}$$

18

The bracket in the above equation emphasizes that ζ should be an integer number. k is a constant which depends on the material. For aluminum, k can be considered as 4 or 6 depending on the alloy. Gambin suggested that in order to obtain a reasonable prediction for texture, the following approximate relation must be considered between the power of the yield function, n, and stacking fault energy (SFE):

$$n \cong \frac{\Gamma}{Gb} \times 10^{-3}$$

(3.10)

where Γ is a value of SFE, G is the shear modulus, and b is the burger's vector.

Based on this formulation n^* can be found as:

$$n^* = \frac{n}{2} \cong \frac{\Gamma}{2Gb} \times 10^{-3}$$

(3.11)

CHAPTER 4

DUAL MIXED MODELS

4.1 Nonsmooth Multi Yield Surface Theory for Crystal Plasticity

According to the nonsmooth multi yield surface theory (Naghdi(1960), Koiter(1953), Nemaat Naser (1983), Simo and Hughes (1998)) the yield surface is composed of several smooth yield surfaces which intersect nonsmoothly. This theory was initially developed for soil and rock mechanics such as; Cam-Clay model, the cap model, and Mohr-Coulomb model. For more information about these models one should look at Loret and Prevost (1986), DiMaggio and Sandler (1971), Sandler and Rubin (1979), Resende and Martin (1986). In plasticity, the classical Tresca yield function is an example of nonsmooth multi yield surface.

Before going further, let us define two very important vectors, q and α, which are frequently used in the theory of plasticity. q is a matrix containing state variables such as back stress and the yield stress and α is a vector containing internal variables such as effective plastic strain. For the simple case of rate independent plasticity with isotropic hardening at room temperature, q would only have one variable, which is the flow stress, $\bar{\sigma}$, and α would have one variable, which is the effective plastic strain, $\bar{\varepsilon}^p$. Now with these definitions let us consider the problem of crystal plasticity as a nonsmooth multi yield surface problem. In a single crystal, depending on the crystal structure, there are several slip systems that can be activated separately. Here we assume that the deformation occurs near room temperature, and that when the resolved shear stress on a slip plane exceeds a critical value plastic deformation

happens. Based on this definition a nonsmooth multi yield surface for a single crystal can be defined mathematically as (Figure 4.1):

$$\partial E_\sigma = \left\{ (\boldsymbol{\sigma}, \mathbf{q}) \mid f_\alpha(\boldsymbol{\sigma}, \mathbf{q}) = 0 \qquad for\ some\ \ \alpha \in [1, 2, ..., N] \right\}$$

(4.1)

and the elastic domain is defined as:

$$E_\sigma = \left\{ (\boldsymbol{\sigma}, \mathbf{q}) \mid f_\alpha(\boldsymbol{\sigma}, \mathbf{q}) \le 0 \qquad for\ all\ \ \alpha \in [1, 2, ..., N] \right\}$$

(4.2)

where N is the number of slip systems.
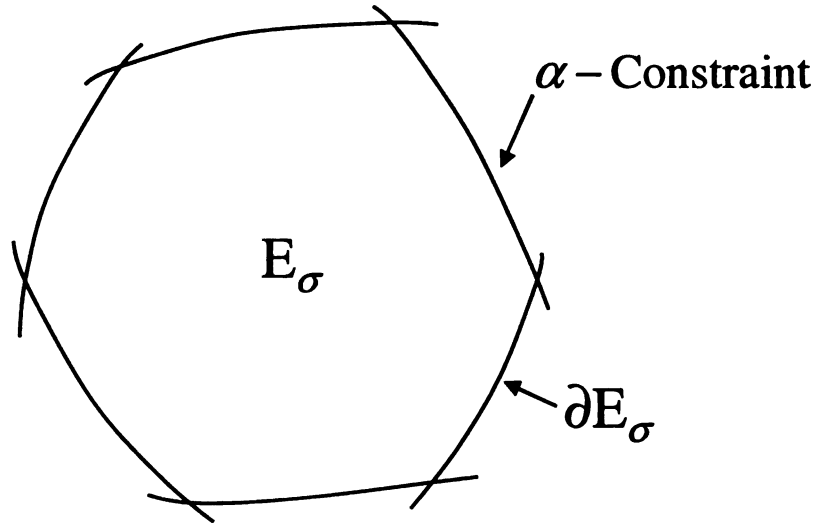
Figure 4.1 Elastic domain in the multi surface plasticity model

With these definitions, the rate of plastic deformation is obtained by:

$$\mathbf{D}^p = \sum_{\alpha=1}^{N} \lambda^\alpha \partial_\sigma f_\alpha(\boldsymbol{\sigma}, \mathbf{q})$$

(4.3)

where $\partial_\sigma f_\alpha(\boldsymbol{\sigma}, \mathbf{q})$ represents differentiation of the yield surface with respect to stress, and λ^α are Lagrange multipliers that are called the plastic consistency parameters in plasticity.

Now with the above definition, let us write the model in a computational format. Any computational problem can be expressed as an optimization problem. The most important part of an optimization problem is to define (an) appropriate objective function(s). Elastic strain energy has been known to be a good objective function for mechanical analysis. For the case of plasticity, a good objective function can be considered to be the simultaneous minimization of the elastic stored energy and the maximization of the release of energy (dissipation) due to plastic work. In other words, an equilibrium must be achieved between the increase in the internal energy due to elastic stored energy of the material and the release of the energy due to the plastic work (Figure 4.2). This is known as the principle of the maximum plastic dissipation (see Mandel (1964) and Lubliner (1984, 1986)). The elastic stored energy W can be expressed as:

$$W^e = \frac{1}{2}\left(\boldsymbol{\varepsilon} - \boldsymbol{\varepsilon}^p\right) : \mathbf{C} : \left(\boldsymbol{\varepsilon} - \boldsymbol{\varepsilon}^p\right)$$

(4.4)

Based on above equation the elastic stiffness matrix, $\mathbf{C}$ is obtained by:

$$C = \frac{\partial^2 W\left(\varepsilon - \varepsilon^p\right)}{\partial\left(\varepsilon - \varepsilon^p\right)^2} \tag{4.5}$$

There is also the following relationship between the elastic stress and strain:

$$\boldsymbol{\sigma} = \nabla W(\boldsymbol{\varepsilon} - \boldsymbol{\varepsilon}^p) = \mathbf{C} : (\boldsymbol{\varepsilon} - \boldsymbol{\varepsilon}^p) \tag{4.6}$$

One can develop a similar function as a measure of the plastic work or dissipation, which is the so called hardening potential, as:

$$\Pi = \frac{1}{2}\mathbf{D} : (\boldsymbol{\alpha} \otimes \boldsymbol{\alpha}) \tag{4.7}$$

where **D** is the so called matrix of generalized plastic moduli and is defined by:

$$\mathbf{D} = \frac{\partial^2 \Pi(\boldsymbol{\alpha})}{\partial \boldsymbol{\alpha}^2} \tag{4.8}$$

State variables are related to the internal variables by:

$$\mathbf{q} = -\nabla \Pi(\boldsymbol{\alpha}) = -\mathbf{D}\boldsymbol{\alpha} \tag{4.9}$$

As explained before, for the simple case of rate independent plasticity with isotropic hardening at room temperature $q = -\bar{\sigma}$ and $\alpha = \bar{\varepsilon}^p$ and one may define the strain hardening as $\bar{\sigma} = k\left(\bar{\varepsilon}^p\right)^n$ or $q = -k(\alpha)^n$. Then, D is a matrix with a single variable as $D = k\alpha^{n-1}$.

In a plasticity problem, the aim is to find the stress tensor and the state variable vector. In other words, the objective function must be defined in such a way that the design variables are stresses. Therefore, for any of the above functions, it is possible

to define a complementary function such as the complementary elastic stored energy potential, $\chi(\sigma)$, and the complementary hardening potential, $\Lambda(q)$, associated with $W(\varepsilon - \varepsilon^p)$ and $\Pi(\alpha)$, respectively. For this case the following relations can be expressed:

$$\mathbf{C}^{-1} = \frac{\partial^2 \chi(\sigma)}{\partial \sigma^2} \tag{4.10}$$

$$\varepsilon^e = \frac{\partial \chi(\sigma)}{\partial \sigma} \tag{4.11}$$

where $\varepsilon^e = \varepsilon - \varepsilon^p$ and

$$\mathbf{D}^{-1} = \frac{\partial^2 \Lambda(q)}{\partial q^2} \tag{4.12}$$

$$\alpha = -\frac{\partial \Lambda(q)}{\partial q} \tag{4.13}$$

With the above definitions, in a plasticity problem, the objective is to minimize the elastic stored potential and at the same time maximize the plastic dissipation. Or, to minimize the difference between the elastic stored energy and the plastic dissipation as:

24

$$(\boldsymbol{\sigma}, \mathbf{q}) = \underset{\boldsymbol{\Sigma}, \mathbf{q} \in \mathbf{E}_\sigma}{Min} \left[\chi(\boldsymbol{\Sigma}) - \Lambda(\mathbf{q}) \right]$$

$$= \underset{\boldsymbol{\Sigma}, \mathbf{q} \in \mathbf{E}_\sigma}{Min} \left[\frac{1}{2} \boldsymbol{\Sigma} : \mathbf{C}^{-1} : \boldsymbol{\Sigma} - \frac{1}{2} \mathbf{q} \cdot \boldsymbol{\alpha} \right]$$

$$= \underset{\boldsymbol{\Sigma}, \mathbf{q} \in \mathbf{E}_\sigma}{Min} \left[\frac{1}{2} \boldsymbol{\Sigma} : \mathbf{C}^{-1} : \boldsymbol{\Sigma} + \frac{1}{2} \mathbf{q} : \mathbf{D}^{-1} : \mathbf{q} \right] \qquad (4.14)$$

Where $\mathbf{E}_\sigma$ is defined in equation (4.2). One should notice that the matrix $\mathbf{D}$ is not constant and is usually a function of $\boldsymbol{\alpha}$.

Now the problem of crystal plasticity can be easily defined. For a given increment and a given stress tensor, $\boldsymbol{\Sigma}$, at the start of the increment (the design variable), and the internal variable vector, $\mathbf{q}$, the crystal plasticity problem is the argument (solution) of the following constrained minimization problem. In the following, the first part of the objective function expresses the elastic stored energy and the second part shows the dissipation of the energy due to plastic deformation.

$$(\boldsymbol{\sigma}_{n+1}, \mathbf{q}_{n+1}) = ARG \left\{ \begin{array}{c} Min[\frac{1}{2}\left(\boldsymbol{\sigma}_{n+1}^{trial} - \boldsymbol{\Sigma}\right) : \mathbf{C}^{-1} : \left(\boldsymbol{\sigma}_{n+1}^{trial} - \boldsymbol{\Sigma}\right) + \\ \frac{1}{2}(\mathbf{q}_n - \mathbf{q}) : \mathbf{D}^{-1} : (\mathbf{q}_n - \mathbf{q})] \\ Subject\ to: \\ f_\alpha(\boldsymbol{\Sigma}, \mathbf{q}) \leq 0 \quad for\ all\ \alpha s \end{array} \right\} \qquad (4.15)$$

25
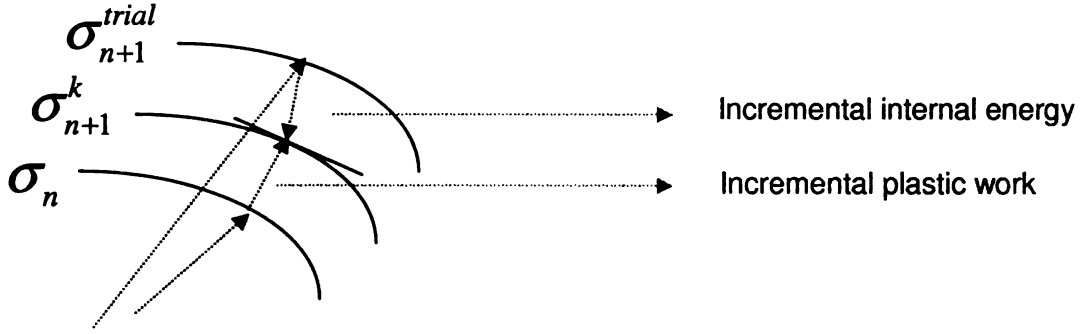
Figure 4.2 The schematic of the competition between elastic stored energy and the plastic work in a plasticity problem

As explained before, the components of **q** vector define the back stress for kinematic hardening or the effective stress for the hardening rule. **C** is the anisotropic elastic stiffness matrix and **D** is the matrix of generalized plastic moduli. σ_{n+1}^{trial} is the trial stress tensor obtained by assuming that all the incremental deformation in a given increment is initially elastic. For a crystal plasticity problem with isotropic hardening, $f_\alpha(\sigma, \mathbf{q})$ is defined as:

$$f_\alpha(\sigma, q) = \frac{\left|\sigma : \mathbf{P}^\alpha\right|}{\tau_y^\alpha(\mathbf{q})} - 1 \tag{4.16}$$

A comparison of equations (2.8), (4.3), and (4.16) shows that for the case of crystal plasticity, λ^α are the same as plastic shear deformations on slip system, $\dot{\gamma}^\alpha$.

4.2 Dual Mixed Model and its Applications to Micromechanics

Due to the interdependency of shear slips $\dot{\gamma}^{\alpha}$, solution to the equation (4.15) for a crystal plasticity problem is usually singular or ill-conditioned, especially for the rate independent case. Several algorithms have been used to overcome this singularity, such as the singular value decomposition method, methods of generalized inverse of the local Jacobian of the active yield criterion functions in reduced space, and the diagonal shift method of the local jacobian matrix (See Kothari and Anand (1996) and Guitino and Ortiz (1992)).

Though the preliminary results of above methods appeared to be effective, further evaluation of them showed that either they are very expensive or unable to overcome the problem arising from singularity or ill-conditioning in more complex strain paths. A new method is introduced in this work which is faster and more efficient, compared with existing methods. This new method is termed as "Dual mixed method". The method is based on a novel mathematical technique that allows us to bridge between the computational mechanics, mathematics, or plasticity and the dislocation theory. Based on this method, in any constrained optimization problem with several constraints, instead of solving for several Lagrange multipliers directly, one may find (an) intermediate function(s) that can be called "duality function(s)" and solve for (a) Lagrange multiplier(s), which can be called "primary Lagrange multiplier(s)", using duality function(s). Then the design variables, state variables, and all Lagrange multipliers of the problem can be obtained using the primary Lagrange multiplier(s) and the duality function(s), indirectly. The duality function(s) can be developed using existing empirical, experimental, mathematical, or physical based relationship

between design and state variables. Although this method is proposed for a crystal plasticity problem, it can be used for any other type of constrained optimization problem. Figure 4.3 shows the schematic of the dual mixed model for solving a constrained optimization problem.

$$\begin{cases} Min\ [\,g(\mathbf{x})\,] \\ Subject\ to:\ \ f_i(\mathbf{x}) \le 0 \quad for\ i = 1,...m \end{cases}$$

Direct Solution

Or using dual mixed method

Develop duality function(s)

Solve for λ_i

Solve for primary Lagrange multiplier(s);

γ_j, $j = 1,...k$

Compute design and state variables

Figure 4. 3 Schematic of dual mixed model for a constrained optimization

4.3. Crystal Plasticity Based on Dual Mixed Model

The kinetics of the dislocations or the dynamic behavior of the dislocation under external loads has been a subject of interest for a long time. A brief and good review on dislocation dynamics can be found in Meyers' book (1984) on mechanical metallurgy. The first study on this subject may be related to the Gilman and

28

Johnston's work (1957, 1959) in measuring the dislocations velocity in LiF. They found a relationship between the velocities of dislocations and the shear stress (Figure 4.4). The following works by other investigators showed that for other materials, the dislocation velocity is also a function of resolved shear stress. Some of these investigations are: Stein and Low for Fe-Si; Ney et al. for Cu and Cu-Al; Schadler for W; Chaudhuri et al. for Ge and Si; Erickson for Fe-Si; Gutmanas et al. for NaCl; Rohde and Pitt for Ni; Pope et al. for Zn; Greenman et al. for Copper; Suzuki and Ishii for Copper; Blish and Vreeland for Zn; Gorman et al. for aluminum; Parameswaran and Weertman for Pb; and Parameswaran et al. for aluminum. Figure (4.5) shows some results of these studies for different materials.
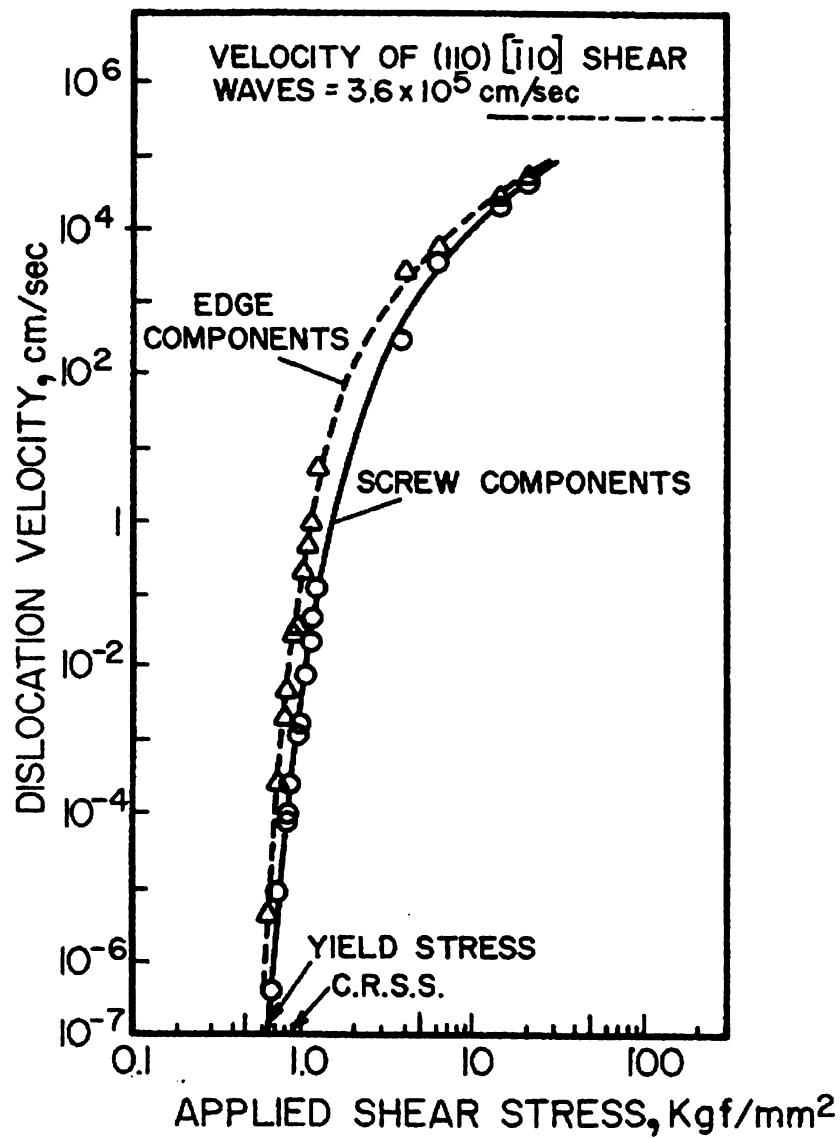
Figure 4.4 Dislocation velocity versus resolved shear stress for LiF single crystal [Johnston and Gilman (1959)]
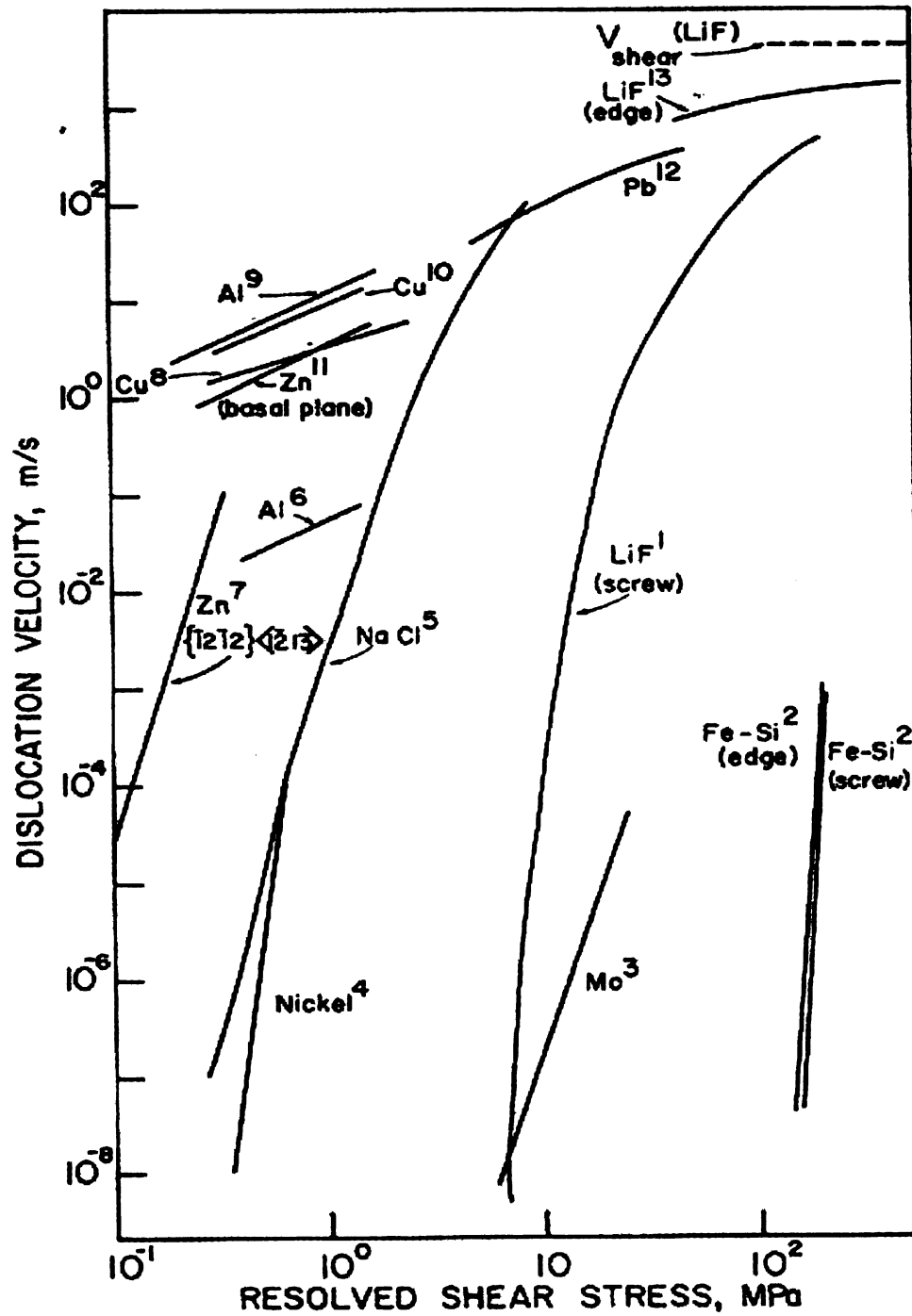
Figure 4.5 Dislocation velocity versus resolved shear stress for different single crystals [Mechanical Metallurgy, Meyers (1984)]

31

Based on the above discussion, the theory of dislocation dynamics has been used to develop a novel crystal plasticity model based on dual mixed model. For this purpose, the duality function of the dual mixed crystal plasticity problem is obtained by using the existing relations in dislocation dynamics theory, which expresses the average velocity of dislocations as a function of resolved shear stress in a single crystal.

Assume that dislocations travel an average distance $\bar{l}$ on slip system α. Then, the plastic shear strain on slip system α is expressed by:

$$\gamma^\alpha = \phi^\alpha \rho^\alpha b^\alpha \bar{l}^{\,\alpha} \tag{4.17}$$

where ϕ^α is a correction factor taking into account the effect of activation of the different independent slip systems, ρ^α is the dislocation density, and b^α is Burgers vector.

The rate of shear strain then is:

$$\dot{\gamma}^\alpha = \phi^\alpha \rho^\alpha b^\alpha \bar{V}^\alpha \tag{4.18}$$

where $\bar{V}^\alpha$ is the average dislocation velocity on slip system α.

The average velocities of dislocations on a slip system may be expressed generally as (Gilman 1962):

$$\bar{V}^\alpha = V_0^\alpha f_p(\tau^\alpha)$$

where V_0^α is the limiting velocity and $f_p(\tau^\alpha)$ is the average probability for dislocations to have a velocity V_0^α at given instant. There have been several

investigations, as explained in the first paragraph of section 4.3, to find $f_p(\tau^\alpha)$ for

different materials. Based on the overall study of all these works, one may classify

$f_p(\tau^\alpha)$ in three different groups; power type average probability functions,

exponential type average probability functions, and average probability function

based on a linear combination of exponential functions (Gilman model). In the

following sections the proposed dual mixed crystal plasticity models based on these

three different dislocation velocity functions will be explained.

4.3.1. Power Type Dual Mixed Crystal Plasticity Model

Johnston and Gilman (1957 and 1959), Hahn (1962), and Greenman (1967) found the

following relationship between the dislocation velocity and resolved shear stress at a

constant temperature:

$$V = V_o \left(\frac{\tau}{\tau_o} \right)^m \qquad\qquad (4.19)$$

where τ_o and V_o are material constants.

Further investigations by Greenman et al. (1967), Pope et al. (1967), Gorman et al.

(1969), and Weertman et al. (1971 and 1972) showed a linear relationship between

the dislocation velocity and resolved shear stress for most of metals (Figure 4.5):

$$V = V_o \left(\frac{\tau}{\tau_o} \right) \qquad\qquad (4.20)$$

and for the case of varying temperature:

33

$$V = V_o \left(\frac{\tau}{\tau_o} \right) \exp \left(-\frac{Q}{KT} \right) \qquad (4.21)$$

where Q is the activation energy, K is the Boltzmann constant, and T is the material temperature in Kelvin. It must be mentioned that the goal of this work is not to develop a temperature sensitive crystal plasticity model. Nevertheless, because its formulation is very similar to a non-temperature sensitive dual mixed crystal plasticity model, it will be covered here but will not be tested or validated and remains open for further researches.

Based on the above observation, we assume that for a small strain increment the average velocity of dislocations on active slip system α can be obtained by:

$$\overline{V}^\alpha = V_o^\alpha \left(\frac{\tau^\alpha}{\tau_y^\alpha} \right)^m \, \mathrm{sgn}(\tau^\alpha) \qquad (4.22)$$

where τ_y^α is the critical resolved shear stress.

For the temperature sensitive case:

$$\overline{V}^\alpha = V_o^\alpha \left(\frac{\tau^\alpha}{\tau_y^\alpha} \right)^m \exp \left(-\frac{Q^\alpha}{KT} \right) \mathrm{sgn}(\tau^\alpha) \qquad (4.23)$$

Combination of equations (4.22) and (4.18) gives:

$$\dot{\gamma}^\alpha = \phi^\alpha \rho^\alpha b^\alpha V_o^\alpha \left(\frac{\tau^\alpha}{\tau_y^\alpha} \right)^m \, \mathrm{sgn}(\tau^\alpha) \qquad (4.24)$$

And for the temperature sensitive case:

$$\dot{\gamma}^{\alpha} = \phi^{\alpha}\rho^{\alpha}b^{\alpha}v_{\circ}^{\alpha}\left(\frac{\tau^{\alpha}}{\tau_{y}^{\alpha}}\right)^{m}\exp\left(-\frac{Q^{\alpha}}{KT}\right)\text{sgn}(\tau^{\alpha}) \tag{4.25}$$

Combination of equations (4.24) and (2.8) yields:

$$\mathbf{D}^{p} = \sum_{\alpha=1}^{N}\phi^{\alpha}\rho^{\alpha}b^{\alpha}v_{\circ}^{\alpha}\left(\frac{\tau^{\alpha}}{\tau_{y}^{\alpha}}\right)^{m}\text{sgn}(\tau^{\alpha})\mathbf{P}^{\alpha} \tag{4.26}$$

and in the same manner substituting for the shear strain rate from equation (4.24) into equation (2.9) yields:

$$\mathbf{\Omega}^{p} = \sum_{\alpha=1}^{N}\phi^{\alpha}\rho^{\alpha}b^{\alpha}v_{\circ}^{\alpha}\left(\frac{\tau^{\alpha}}{\tau_{y}^{\alpha}}\right)^{m}\text{sgn}(\tau^{\alpha})\mathbf{w}^{\alpha} \tag{4.27}$$

Assuming that $\lambda = \phi^{\alpha}\rho^{\alpha}b^{\alpha}v_{\circ}^{\alpha}\dfrac{\tau_{y}^{\alpha}}{n}\left(\dfrac{\tau^{\alpha}}{\tau_{y}^{\alpha}}\right)^{n_{1}}$ parameter is the same for all slip systems, one can rewrite equations (4.26) and (4.27) as:

$$\mathbf{D}^{p} = \lambda\sum_{\alpha=1}^{N}\frac{n}{\tau_{y}^{\alpha}}\left(\frac{\tau^{\alpha}}{\tau_{y}^{\alpha}}\right)^{n_{2}}\text{sgn}(\tau^{\alpha})\mathbf{P}^{\alpha} \tag{4.28}$$

$$\mathbf{\Omega}^{p} = \lambda\sum_{\alpha=1}^{N}\frac{n}{\tau_{y}^{\alpha}}\left(\frac{\tau^{\alpha}}{\tau_{y}^{\alpha}}\right)^{n_{2}}\text{sgn}(\tau^{\alpha})\mathbf{w}^{\alpha} \tag{4.29}$$

where $m=n_{1}+n_{2}$ and $n=n_{2}+1$.

According to the normality rule in plasticity, a potential $f(\sigma,q)$ can be considered in such a way that:

$$\mathbf{D}^p = \lambda \partial_\sigma f(\mathbf{\sigma}, \mathbf{q}) \tag{4.30}$$

Comparing equation (4.30) with (4.28) one can easily find the following relation for active slip systems:

$$\partial_\sigma f(\mathbf{\sigma}, \mathbf{q}) = \sum_{\alpha=1}^{N} \frac{n}{\tau_y^\alpha} \left(\frac{\tau^\alpha}{\tau_y^\alpha} \right)^{n_2} \operatorname{sgn}(\tau^\alpha) \mathbf{P}^\alpha \tag{4.31}$$

Or

$$f(\mathbf{\sigma}, \mathbf{q}) = \sum_{\alpha=1}^{N} \left(\frac{|\mathbf{\sigma} : \mathbf{P}^\alpha|}{\tau_y^\alpha} \right)^n + h(\mathbf{q}, N) \quad \text{for } N \text{ active slip systems} \tag{4.32}$$

In a similar manner one can easily derive a function for temperature sensitive case:

$$g(\mathbf{\sigma}, \mathbf{q}, T) = \sum_{\alpha=1}^{N} \left(\frac{|\mathbf{\sigma} : \mathbf{P}^\alpha|}{\tau_y^\alpha} \right)^n \exp\left(-\frac{Q^\alpha}{KT} \right) + h(N, \mathbf{q}, T) \tag{4.33}$$

$$\text{for } N \text{ active slip systems}$$

And the rate of plastic deformation and spin for the temperature sensitive case are:

$$\mathbf{D}^p = \lambda \sum_{\alpha=1}^{N} \frac{n}{\tau_y^\alpha} \left(\frac{\tau^\alpha}{\tau_y^\alpha} \right)^{n_2} \exp\left(-\frac{Q^\alpha}{KT} \right) \operatorname{sgn}(\tau^\alpha) \mathbf{P}^\alpha \tag{4.34a}$$

$$\mathbf{\Omega}^p = \lambda \sum_{\alpha=1}^{N} \frac{n}{\tau_y^\alpha} \left(\frac{\tau^\alpha}{\tau_y^\alpha} \right)^{n_2} \exp\left(-\frac{Q^\alpha}{KT} \right) \operatorname{sgn}(\tau^\alpha) \mathbf{w}^\alpha \tag{4.34b}$$

With the above procedure, two duality functions for crystal plasticity problem (4.15) were found. The first one, equation (4.32), is for constant temperature and the second one, equation (4.33), is temperature sensitive. λ is the primary Lagrange multiplier. To complete the dual mixed crystal plasticity problem, a relation between the primary Lagrange multiplier and the Lagrange multipliers of the crystal plasticity problem (4.15), which are $\dot{\gamma}^{\alpha}$s, must be found. Rewriting equations (4.24) and (4.25) by substituting for λ in these equations, the following expressions for $\dot{\gamma}^{\alpha}$ can be found:

$$\dot{\gamma}^{\alpha} = \lambda \frac{n}{\tau_y^{\alpha}} \left(\frac{\tau^{\alpha}}{\tau_y^{\alpha}} \right)^{n_2} \mathrm{sgn}(\tau^{\alpha})$$

(4.35a)

and for temperature sensitive case:

$$\dot{\gamma}^{\alpha} = \lambda \frac{n}{\tau_y^{\alpha}} \left(\frac{\tau^{\alpha}}{\tau_y^{\alpha}} \right)^{n_2} \exp\left(-\frac{Q^{\alpha}}{KT} \right) \mathrm{sgn}(\tau^{\alpha})$$

(4.35b)

One may use the concept of the plastic work to find a general relationship between the duality function, primary Lagrange multiplier, and the Lagrange multipliers of the problem, $\dot{\gamma}^{\alpha}$. The rate of the plastic work is expressed by:

$$\dot{w} = \mathbf{D}^p : \boldsymbol{\sigma} = \lambda \frac{\partial f}{\partial \boldsymbol{\sigma}} : \boldsymbol{\sigma} = \lambda \sum_{\alpha=1}^{N} \frac{\partial f}{\partial \tau^{\alpha}} \frac{\partial \tau^{\alpha}}{\partial \boldsymbol{\sigma}} : \boldsymbol{\sigma} = \lambda \sum_{\alpha=1}^{N} \frac{\partial f}{\partial \tau^{\alpha}} \tau^{\alpha}$$

(4.36)

37

And also the rate of the plastic work in a single crystal can be obtained using slip rates as:

$$\dot{w} = \sum_{\alpha=1}^{N} \dot{\gamma}^{\alpha} \tau^{\alpha} \tag{4.37}$$

Comparing the above equations, the following expression for the rate of slip shear, $\dot{\gamma}^{\alpha}$, can be found:

$$\dot{\gamma}^{\alpha} = \lambda \partial_{\tau^{\alpha}} f(\boldsymbol{\sigma}, \mathbf{q}) \tag{4.38}$$

Now in crystal plasticity problem shown in (4.15), instead of using several constraints $f_{\alpha}(\boldsymbol{\sigma}, \mathbf{q}) \leq 0$ for all slip systems one can use a single duality function $f(\boldsymbol{\sigma}, \mathbf{q}) \leq 0$ shown in equation (4.32) to find the primary Lagrange multiplier and then rate of slip shears, $\dot{\gamma}^{\alpha}$ s, as discussed above. This overcomes the problem arising from ill-conditioning and computational intensity.

4.3.2. Exponential Type Dual Mixed Crystal Plasticity Model

Rohde and Pitt (1967) found that a good correlation for the relationship between dislocations velocity and stress could be obtained using an exponential type equation for the average probability function. Based on theoretical calculation they found the following expression for the average dislocations velocity:

$$\overline{V} = \frac{kT}{h} K \exp\left(-\frac{\Delta H}{kT}\right) \exp\left[\frac{B(\tau_a - \tau_l)}{kT}\right] \tag{4.39}$$

where h is the Plank's constant, K a numerical constant, B an activation volume, ΔH the enthalpy of activation, τ_a the applied resolved shear stress, and τ_l the long-range internal stress.

For any slip system the above equation can be rewritten as:

$$\overline{V}^\alpha = \frac{kT}{h} K^\alpha \exp\left(-\frac{\Delta H}{kT}\right)\exp\left[\frac{B^\alpha(\tau^\alpha - \tau_l^\alpha)}{kT}\right]$$

(4.40)

Utilizing the above equation, a plot of $\log V$ vs τ^α at constant temperature should yield a straight line with a slope of $\frac{B}{2.3kT}$ if it is assumed that B is not a function of the applied stress. If B is a function of the applied stress, then the plot would not be a straight line. For most metals, as can been seen from Figure 4.5, dislocations velocity is a linear function of the applied stress and B remains almost constant over the range of applied stresses.

In a strain increment for a constant temperature case, equation (4.40) can also be written as:

$$\overline{V}^\alpha = K'^\alpha \exp\left[C'^\alpha\left(\left|\tau^\alpha\right| - \tau_y^\alpha\right)\right]\text{sgn}(\tau^\alpha)$$

(4.41)

where τ_y^α is the critical shear stress on slip system α.

Although the above equation correlates very well with the experimental data, it is not in a suitable format for a computational algorithm. When it is used in the above format in a computational algorithm it causes stability problems. A better way of expressing equation (4.41) is to modify as following:

For active slip systems $|\tau^\alpha| - \tau_y^\alpha \geq 0$ or $\dfrac{|\tau^\alpha|}{\tau_y^\alpha} - 1 \geq 0$ and also $\dfrac{|\tau^\alpha|}{\tau_y^\alpha} \geq 0$, one can

also fit the experimental data using the following equations:

$$\overline{V}^\alpha = K_1^\alpha \exp\left[C_1^\alpha \left(\frac{|\tau^\alpha|}{\tau_y^\alpha} - 1 \right) \right] \operatorname{sgn}(\tau^\alpha) \tag{4.42}$$

Or

$$\overline{V}^\alpha = K_2^\alpha \exp\left(C_2^\alpha \frac{|\tau^\alpha|}{\tau_y^\alpha} \right) \operatorname{sgn}(\tau^\alpha) \tag{4.43}$$

Then using equation (4.18), the rate of slip on any slip system is expressed by:

$$\dot{\gamma}^\alpha = \phi^\alpha \rho^\alpha b^\alpha K_1^\alpha \exp\left[C_1^\alpha \left(\frac{|\tau^\alpha|}{\tau_y^\alpha} - 1 \right) \right] \operatorname{sgn}(\tau^\alpha) \tag{4.44}$$

and the rate of plastic deformation is obtained by:

$$\mathbf{D}^p = \sum_{\alpha=1}^{N} \phi^\alpha \rho^\alpha b^\alpha K_1^\alpha \exp\left[C_1^\alpha \left(\frac{|\tau^\alpha|}{\tau_y^\alpha} - 1 \right) \right] \operatorname{sgn}(\tau^\alpha) \mathbf{P}^\alpha \tag{4.45}$$

Again let us assume that $\lambda = \phi^\alpha \rho^\alpha b^\alpha k_1^\alpha G(\tau^\alpha, \tau_y^\alpha)$ is the same for all slip

systems. Knowing $\tau^\alpha = \boldsymbol{\sigma} : \mathbf{P}^\alpha$, then equation (4.45) can be rewritten as:

$$\mathbf{D}^p = \lambda \sum_{\alpha=1}^{N} \frac{C^\alpha}{\tau_y^\alpha} \exp\left[C^\alpha \left(\frac{|\boldsymbol{\sigma} : \mathbf{P}^\alpha|}{\tau_y^\alpha} - 1 \right) \right] \operatorname{sgn}(\tau^\alpha) \mathbf{P}^\alpha \tag{4.46}$$

and spin can be expressed by:

40

$$\mathbf{\Omega}^p = \lambda \sum_{\alpha=1}^{N} \frac{C^{\alpha}}{\tau_y^{\alpha}} \exp\left[C^{\alpha} \left(\frac{|\boldsymbol{\sigma} : \mathbf{P}^{\alpha}|}{\tau_y^{\alpha}} - 1 \right) \right] \operatorname{sgn}(\tau^{\alpha}) \mathbf{w}^{\alpha} \tag{4.47}$$

Assuming that the associative flow rule can be used here, by comparing equations (2.8), (4.30), and (4.46) one can find the following relationship:

$$\partial_{\sigma} f(\boldsymbol{\sigma}, \mathbf{q}) = \sum_{\alpha=1}^{N} \frac{C^{\alpha}}{\tau_y^{\alpha}} \exp\left[C^{\alpha} \left(\frac{|\boldsymbol{\sigma} : \mathbf{P}^{\alpha}|}{\tau_y^{\alpha}} - 1 \right) \right] \operatorname{sgn}(\tau^{\alpha}) \mathbf{P}^{\alpha} \tag{4.48}$$

Then a duality function for the crystal plasticity problem (4.15) can be obtained as:

$$f(\boldsymbol{\sigma}, \mathbf{q}) = \sum_{\alpha=1}^{N} \exp\left[C^{\alpha} \left(\frac{|\boldsymbol{\sigma} : \mathbf{P}^{\alpha}|}{\tau_y^{\alpha}} - 1 \right) \right] + h_1(N, \mathbf{q}) \tag{4.49}$$

for N active slip systems

The relationship between the primary Lagrange multiplier λ and the Lagrange multipliers of the crystal plasticity problem $\dot{\gamma}^{\alpha}$s is given by equation (4.38) as:

$$\dot{\gamma}^{\alpha} = \lambda \frac{C^{\alpha}}{\tau_y^{\alpha}} \exp\left[C^{\alpha} \left(\frac{|\boldsymbol{\sigma} : \mathbf{P}^{\alpha}|}{\tau_y^{\alpha}} - 1 \right) \right] \operatorname{sgn}(\tau^{\alpha}) \tag{4.50}$$

And by following the same procedure for equation (4.43) one can obtain the following duality function:

$$g(\boldsymbol{\sigma}, \mathbf{q}) = \sum_{\alpha=1}^{N} \exp\left[D^{\alpha} \left(\frac{|\boldsymbol{\sigma} : \mathbf{P}^{\alpha}|}{\tau_y^{\alpha}} \right) \right] + h_2(N, \mathbf{q}) \tag{4.51}$$

for N active slip systems

The rate of the plastic deformation is given by:

$$\mathbf{D}^p = \lambda \sum_{\alpha=1}^{N} \frac{D^\alpha}{\tau_y^\alpha} \exp\left[D^\alpha \left(\frac{|\boldsymbol{\sigma} : \mathbf{P}^\alpha|}{\tau_y^\alpha} \right) \right] \operatorname{sgn}(\tau^\alpha) \mathbf{P}^\alpha \tag{4.52}$$

And the plastic spin is obtained by:

$$\boldsymbol{\Omega}^p = \lambda \sum_{\alpha=1}^{N} \frac{D^\alpha}{\tau_y^\alpha} \exp\left[D^\alpha \left(\frac{|\boldsymbol{\sigma} : \mathbf{P}^\alpha|}{\tau_y^\alpha} \right) \right] \operatorname{sgn}(\tau^\alpha) \mathbf{w}^\alpha \tag{4.53}$$

The Lagrange multipliers of the crystal plasticity problem are obtained by:

$$\dot{\gamma}^\alpha = \lambda \frac{D^\alpha}{\tau_y^\alpha} \exp\left[D^\alpha \left(\frac{|\boldsymbol{\sigma} : \mathbf{P}^\alpha|}{\tau_y^\alpha} \right) \right] \operatorname{sgn}(\tau^\alpha) \tag{4.54}$$

It will be shown in the next chapters that with proper selection of functions h_1 and h_2 in equations (4.49) and (4.51), the coefficients C^α and D^α are the same.

With the above duality functions and relations showing the relationship between primary Lagrange multiplier and the Lagrange multipliers of the crystal plasticity problem, the exponential type dual mixed crystal plasticity problem is complete.

4.3.3. Dual Mixed Crystal Plasticity Model Based on Gilman's Dislocation Velocity Model

For any crystal structure, the dislocation velocity cannot increase without a bound as stresses increase because there are always loss mechanisms present in any real crystal. The dislocation velocity must saturate below the velocity of the sound wave under a continuous stress field.

The average probability function $f_p(\tau^\alpha)$ must have a zero value when $\tau^\alpha = 0$, and must approach unity for large τ^α. Gilman (1969) proposed a probability function that has these limits:

$$f_p(\tau) = \exp(-D/\tau) \tag{4.55}$$

where D is the characteristic drag stress. This function gives a good representation of the data at medium to high stress levels. This function also can represent the plastic yielding phenomenon by sudden transition from low to high value when $\tau \cong D/2$. However, it cannot represent the linear velocity-stress relations that are observed in most metals. Also, due to the complicated derivatives it shows a poor form at low-level stresses.

A better probability function that can represent the linear behavior at small stress levels plus saturation at high stress levels is (Gilman 1969):

$$f_p(\tau, s) = 1 - \exp(-\tau/s) \tag{4.56}$$

where s is the coupling stress that acts across the glide plane. For small stress levels this function becomes τ/s. Therefore, the velocity has a linear relationship with stress.

According to Gilman (1969) the behavior of almost any material can be represented by a combination of equations (4.55) and (4.56) as:

$$\overline{V} = V_s^*\left[1 - \exp(-\tau/s)\right] + V_d^* \exp(-D/\tau) \tag{4.57}$$

43

Here two different dual mixed crystal plasticity models are developed based on equations (4.56) and (4.57), respectively.

4.3.3.1. Dual mixed crystal plasticity model based on equation (4.56)

Let us rewrite equation (4.56) as:

$$\bar{V}^\alpha = V_0^\alpha \left[1 - \exp\left(-\frac{|\tau^\alpha|}{\tau_y^\alpha} \right) \right] \mathrm{sgn}(\tau^\alpha) \tag{4.58}$$

Then using equation (4.18) the rate of shear slip on any slip system is expressed by:

$$\dot{\gamma}^\alpha = \phi^\alpha \rho^\alpha b^\alpha V_0^\alpha \left[1 - \exp\left(-\frac{|\tau^\alpha|}{\tau_y^\alpha} \right) \right] \mathrm{sgn}(\tau^\alpha) \tag{4.59}$$

Assuming $\lambda_1 = \phi^\alpha \rho^\alpha b^\alpha V_0^\alpha F_1(\tau^\alpha, \tau_y^\alpha)$ and $\lambda_2 = \phi^\alpha \rho^\alpha b^\alpha V_0^\alpha F_2(\tau^\alpha, \tau_y^\alpha)$

are the same for all slip systems, then equation (4.59) can be written as:

$$\dot{\gamma}^\alpha = \left[\lambda_1 \frac{n}{\tau_y^\alpha} \left(\frac{|\tau^\alpha|}{\tau_y^\alpha} \right)^{n-1} - \lambda_2 \frac{C_3^\alpha}{\tau_y^\alpha} \exp\left(-C_3^\alpha \frac{|\tau^\alpha|}{\tau_y^\alpha} \right) \right] \mathrm{sgn}(\tau^\alpha) \tag{4.60}$$

Substituting for $\dot{\gamma}^\alpha$ in equation (2.8) the rate of plastic deformation is obtained as:

$$\mathbf{D}^p = \sum_{\alpha=1}^{N} \left[\lambda_1 \frac{n}{\tau_y^\alpha} \left(\frac{|\tau^\alpha|}{\tau_y^\alpha} \right)^{n-1} - \lambda_2 \frac{C_3^\alpha}{\tau_y^\alpha} \exp\left(-C_3^\alpha \frac{|\tau^\alpha|}{\tau_y^\alpha} \right) \right] \mathrm{sgn}(\tau^\alpha) \mathbf{P}^\alpha \tag{4.61}$$

Assuming the associative flow rule, equation (4.61) can be rewritten as:

$$\mathbf{D}^p = \lambda_1 \frac{\partial f_1(\tau^\alpha, \tau_y^\alpha)}{\partial \sigma} + \lambda_2 \frac{\partial f_2(\tau^\alpha, \tau_y^\alpha)}{\partial \sigma} \tag{4.62}$$

44

Equation (4.61) shows two primary Lagrange multipliers. Therefore, this problem has two duality functions as follow:

$$f_1(\tau^\alpha, \tau_y^\alpha, N) = \sum_{\alpha=1}^{N} \left(\frac{|\tau^\alpha|}{\tau_y^\alpha} \right)^n + h_1(N, \tau_y^\alpha)$$

(4.63)

And

$$f_2(\tau^\alpha, \tau_y^\alpha, N) = \sum_{\alpha=1}^{N} \exp\left(-C_3^\alpha \frac{|\tau^\alpha|}{\tau_y^\alpha} \right) + h_2(N, \tau_y^\alpha)$$

(4.64)

Although it is possible to solve the dual mixed crystal plasticity model with two duality functions shown above. To simplify the problem one may assume $\lambda_1 = \lambda_2 = \lambda$ and rewrite equation (4.61) as:

$$\mathbf{D}^p = \lambda \sum_{\alpha=1}^{N} \left[\frac{n}{\tau_y^\alpha} \left(\frac{|\tau^\alpha|}{\tau_y^\alpha} \right)^{n-1} - \frac{C_3^\alpha}{\tau_y^\alpha} \exp\left(-C_3^\alpha \frac{|\tau^\alpha|}{\tau_y^\alpha} \right) \right] \operatorname{sgn}(\tau^\alpha) \mathbf{P}^\alpha$$

(4.65)

Assuming associative flow rule, the duality function is obtained as:

$$f(\boldsymbol{\sigma}, \mathbf{q}) = \sum_{\alpha=1}^{N} \left[\left(\frac{|\boldsymbol{\sigma} : \mathbf{P}^\alpha|}{\tau_y^\alpha} \right)^n + \exp\left(-C_3^\alpha \frac{|\boldsymbol{\sigma} : \mathbf{P}^\alpha|}{\tau_y^\alpha} \right) \right] + h(N, \mathbf{q})$$

(4.66)

for N active slip systems

The plastic spin is then expressed by:

$$\boldsymbol{\Omega}^p = \lambda \sum_{\alpha=1}^{N} \left[\frac{n}{\tau_y^\alpha} \left(\frac{|\boldsymbol{\sigma} : \mathbf{P}^\alpha|}{\tau_y^\alpha} \right)^{n-1} - \frac{C_3^\alpha}{\tau_y^\alpha} \exp\left(-C_3^\alpha \frac{|\boldsymbol{\sigma} : \mathbf{P}^\alpha|}{\tau_y^\alpha} \right) \right] \operatorname{sgn}(\tau^\alpha) \mathbf{w}^\alpha$$

(4.67)

And the Lagrange multipliers of the crystal plasticity problem, $\dot{\gamma}^\alpha$, are obtained by:

$$\dot{\gamma}^\alpha = \lambda \left[\frac{n}{\tau_y^\alpha} \left(\frac{|\boldsymbol{\sigma} : \mathbf{P}^\alpha|}{\tau_y^\alpha} \right)^{n-1} - \frac{C_3^\alpha}{\tau_y^\alpha} \exp \left(-C_3^\alpha \frac{|\boldsymbol{\sigma} : \mathbf{P}^\alpha|}{\tau_y^\alpha} \right) \right] \mathrm{sgn}(\tau^\alpha) \qquad (4.68)$$

4.3.3.2. Dual Mixed Crystal Plasticity Model Based on Equation (4.57)

Let us express the Gilman's equation for dislocation velocity shown in equation (4.57) as:

$$\bar{V}^\alpha = \left\{ V_s^\alpha \left[1 - \exp \left(-\frac{|\tau^\alpha|}{\tau_y^\alpha} \right) \right] + V_d^\alpha \exp \left(-\frac{S^\alpha}{|\tau^\alpha|} \right) \right\} \mathrm{sgn}(\tau^\alpha) \qquad (4.69)$$

As mentioned before in equation (4.57), D is a parameter representing the plastic

yielding phenomenon by sudden transition from low to high value when $\tau \simeq D/2$.

S^α has been introduced based on this concept and is assumed that

$$D = S^\alpha = 2\tau_y^\alpha .$$

Slip rate on any slip system is obtained using equation (4.18) by:

$$\dot{\gamma}^\alpha = \phi^\alpha \rho^\alpha b^\alpha v_s^\alpha \left\{ 1 - \exp \left(-\frac{|\tau^\alpha|}{\tau_y^\alpha} \right) + k^\alpha \exp \left(-\frac{S^\alpha}{|\tau^\alpha|} \right) \right\} \mathrm{sgn}(\tau^\alpha) \qquad (4.70)$$

where $k^\alpha = v_d^\alpha / v_s^\alpha$.

Let us assume that there are three primary Lagrange multipliers that are the same for all slip systems and can be expressed as $\lambda_1 = \phi^\alpha \rho^\alpha b^\alpha v_s^\alpha G_1(\tau^\alpha, \tau_y^\alpha)$,

$\lambda_2 = \phi^\alpha \rho^\alpha b^\alpha v_s^\alpha G_2(\tau^\alpha, \tau_y^\alpha)$, and $\lambda_3 = \phi^\alpha \rho^\alpha b^\alpha v_s^\alpha G_3(\tau^\alpha, \tau_y^\alpha)$. Then

equation (4.70) can be expressed as:

$$
\dot{\gamma}^\alpha = \left\{ \lambda_1 \frac{m}{\tau_y^\alpha} \left(\frac{|\tau^\alpha|}{\tau_y^\alpha} \right)^{m-1} - \lambda_2 \frac{C_4^\alpha}{\tau_y^\alpha} \exp\left(-C_4^\alpha \frac{|\tau^\alpha|}{\tau_y^\alpha} \right) + \lambda_3 k^\alpha \frac{C_5^\alpha}{\tau_y^\alpha} \exp\left(-C_5^\alpha \frac{S^\alpha}{|\tau^\alpha|} \right) \right\} \mathrm{sgn}(\tau^\alpha)
$$

$$\text{4.71)}$$

Therefore the rate of the plastic deformation is given as:

$$
\mathbf{D}^P = \sum_{\alpha=1}^{N} \left\{ \lambda_1 \frac{m}{\tau_y^\alpha} \left(\frac{|\tau^\alpha|}{\tau_y^\alpha} \right)^{m-1} - \lambda_2 \frac{C_4^\alpha}{\tau_y^\alpha} \exp\left(-C_4^\alpha \frac{|\tau^\alpha|}{\tau_y^\alpha} \right) + \lambda_3 k^\alpha \frac{C_5^\alpha}{\tau_y^\alpha} \exp\left(-C_5^\alpha \frac{S^\alpha}{|\tau^\alpha|} \right) \right\} \mathrm{sgn}(\tau^\alpha) \mathbf{P}^\alpha
$$

$$\text{(4.72)}$$

Assuming associative flow rule, there are three duality functions in such a way that:

$$
\mathbf{D}^P = \lambda_1 \frac{\partial g_1(\tau^\alpha, \tau_y^\alpha)}{\partial \sigma} + \lambda_2 \frac{\partial g_2(\tau^\alpha, \tau_y^\alpha)}{\partial \sigma} + \lambda_3 \frac{\partial g_3(\tau^\alpha, \tau_y^\alpha)}{\partial \sigma} \tag{4.73}
$$

where

$$
g_1(\tau^\alpha, \tau_y^\alpha, N) = \sum_{\alpha=1}^{N} \left(\frac{|\tau^\alpha|}{\tau_y^\alpha} \right)^m + \psi_1(N, \tau_y^\alpha) \tag{4.74}
$$

and

$$g_2(\tau^\alpha, \tau_y^\alpha, N) = \sum_{\alpha=1}^{N} \exp\left(-C_4^\alpha \frac{|\tau^\alpha|}{\tau_y^\alpha}\right) + \psi_2(N, \tau_y^\alpha) \tag{4.75}$$

and

$$g_3(\tau^\alpha, \tau_y^\alpha, N) = \Upsilon(\tau^\alpha, \tau_y^\alpha, N) + \psi_3(N, \tau_y^\alpha) \tag{4.76}$$

where

$$\Upsilon(\tau^\alpha, \tau_y^\alpha, N) = \sum_{\alpha=1}^{N} k^\alpha \frac{C_5^\alpha}{\tau_y^\alpha} \left\{ |\tau^\alpha| \exp\left(-C_5^\alpha \frac{S^\alpha}{|\tau^\alpha|}\right) + C_5^\alpha S^\alpha \ln\left(\frac{1}{|\tau^\alpha|}\right) + \right.$$
$$\left. \frac{C_5^\alpha S^\alpha}{1 \cdot 1! \cdot |\tau^\alpha|} + \frac{\left(C_5^\alpha S^\alpha\right)^2}{2 \cdot 2! \cdot |\tau^\alpha|^2} + \frac{\left(C_5^\alpha S^\alpha\right)^3}{3 \cdot 3! \cdot |\tau^\alpha|^3} + \cdots \right\} \tag{4.77}$$

Now, the crystal plasticity problem can be solved using the above three duality functions and equations (4.71) and (4.73). To simplify the problem it is assumed that it is possible to find functions G_1, G_2, and G_3 in such a way that $\lambda_1 = \lambda_2 = \lambda_3 = \lambda$. Then equation (4.72) can be rewritten as:

$$\mathbf{D}^P = \lambda \sum_{\alpha=1}^{N} \left\{ \frac{m}{\tau_y^\alpha} \left(\frac{|\boldsymbol{\sigma}:\mathbf{P}^\alpha|}{\tau_y^\alpha}\right)^{m-1} - \frac{C_4^\alpha}{\tau_y^\alpha} \exp\left(-C_4^\alpha \frac{|\boldsymbol{\sigma}:\mathbf{P}^\alpha|}{\tau_y^\alpha}\right) + \right.$$
$$\left. k^\alpha \frac{C_5^\alpha}{\tau_y^\alpha} \exp\left(-C_5^\alpha \frac{\bar{\sigma}_g}{|\boldsymbol{\sigma}:\mathbf{P}^\alpha|}\right) \right\} \operatorname{sgn}(\tau^\alpha) \mathbf{P}^\alpha \tag{4.78}$$

And therefore, the duality function is expressed as:

$$g(\boldsymbol{\sigma},\mathbf{q}) = \sum_{\alpha=1}^{N}\left\{\left(\frac{\left|\boldsymbol{\sigma}:\mathbf{P}^{\alpha}\right|}{\tau_{y}^{\alpha}}\right)^{m} + \exp\left(-C_{4}^{\alpha}\frac{\left|\boldsymbol{\sigma}:\mathbf{P}^{\alpha}\right|}{\tau_{y}^{\alpha}}\right) + \Upsilon(\tau^{\alpha},\tau_{y}^{\alpha},N)\right\} + \psi(N,\mathbf{q})$$

for N active slip systems

(4.79)

The slip rate is defined as a function of the primary Lagrange multiplier as:

$$\dot{\gamma}^{\alpha} = \lambda\left\{\frac{m}{\tau_{y}^{\alpha}}\left(\frac{\left|\boldsymbol{\sigma}:\mathbf{P}^{\alpha}\right|}{\tau_{y}^{\alpha}}\right)^{m-1} - \frac{C_{4}^{\alpha}}{\tau_{y}^{\alpha}}\exp\left(-C_{4}^{\alpha}\frac{\left|\boldsymbol{\sigma}:\mathbf{P}^{\alpha}\right|}{\tau_{y}^{\alpha}}\right) + \right.$$

$$\left. k^{\alpha}\frac{C_{5}^{\alpha}}{\tau_{y}^{\alpha}}\exp\left(-C_{5}^{\alpha}\frac{\overline{\sigma}_{g}}{\left|\boldsymbol{\sigma}:\mathbf{P}^{\alpha}\right|}\right)\right\}\mathrm{sgn}(\tau^{\alpha})$$

(4.80)

With above equations, the dual mixed crystal plasticity model is completely defined for Gilman's dislocation velocity model.

Before closing this chapter, it should be mentioned here that the duality functions are not a yield criterion for a single crystal. In other words, a duality function can not be used as a yield function for a single crystal. They can be only used to find the direction of the plastic flow and also to find the Lagrange multipliers of the problem. The other important point about the duality functions is that they are used for active slip systems. Therefore, to find out about the current yielding situation or the current number of active slip systems in a crystal, one should use equation (4.16) as a yielding criterion.

CHAPTER 5

YIELD SURFACE FOR SINGLE CRYSTALS

5.1. Combined Constraints Method in Constrained Optimization

Another approach to overcome the problem arising from interdependency of plastic slip shears is to use a single yield function for a single crystal. A new yield function for single crystals based on combined constraints method is developed here. According to Kreisselmeier and Steinhauser (1979) for problems with large numbers of inequality constraints, it is possible to construct an equivalent constraint to replace them. Let us consider the following optimization problem with several inequality constraints ($f_i(x) \geq 0$, $i = 1...m$):

$$\begin{cases} Min\ [g(\mathbf{x})] \\ Subject\ to:\ f_i(\mathbf{x}) \geq 0 \quad for\ i = 1,...m \end{cases} \tag{5.1}$$

The following function can then be used as an equivalent single constraint:

$$h(\mathbf{x}) = -\frac{1}{\rho} \ln \left[\sum_i^m \exp\left(-\rho f_i(\mathbf{x})\right) \right] \tag{5.2}$$

Where ρ is a parameter that determines the closeness of the $h(x)$ to the smallest inequality, $min[f_i(\mathbf{x})]$. $h(x)$ is usually called a *KS*-function. For any positive value of ρ, $h(x)$ is always more negative than the most negative constraint, forming a lower band envelop to the equalities. As the value of ρ is increased, $h(x)$ conforms

50

with minimum value of the constraints more closely. The value of $h(\mathbf{x})$ is always bounded by:

$$f_{\min}(\mathbf{x}) \leq h(x) \leq f_{\min}(\mathbf{x}) - \frac{\ln(m)}{\rho} \qquad (5.3)$$

In a same manner one can easily extend the application of the above method for the case when constraints $f_i(\mathbf{x}) \leq 0$, $i = 1...m$. For this case the following function can be used as an equivalent single constraint:

$$h(\mathbf{x}) = \frac{1}{\rho} \ln \left[\sum_i^m \exp(\rho f_i(\mathbf{x})) \right] \qquad (5.4)$$

5.2. A Single Crystal Yield Surface Based on Combined Constraints Method

Let us consider the optimization problem of (4.15) for crystal plasticity problem where the constraints are:

$$f_\alpha(\boldsymbol{\sigma}, \mathbf{q}) = \frac{|\boldsymbol{\sigma} : \mathbf{P}^\alpha|}{\tau_y^\alpha} - 1 \leq 0 \ \ for \ \alpha = 1...N \qquad (5.5)$$

where N is the number of slip systems.

The constraints of (5.5) can be combined using equation (5.4) as:

$$f(\boldsymbol{\sigma}, \mathbf{q}) = \frac{1}{\rho} \ln \left\{ \sum_{\alpha=1}^N \exp \left[\rho \left(\frac{|\boldsymbol{\sigma} : \mathbf{P}^\alpha|}{\tau_y^\alpha} - 1 \right) \right] \right\} \qquad (5.6)$$

Here as the value of ρ is increased, $f(\boldsymbol{\sigma}, \mathbf{q})$ conforms with maximum value of the constraints more closely. The value of $f(\boldsymbol{\sigma}, \mathbf{q})$ is always bounded by:

$$f_{\max}(\mathbf{x}) \le f(\mathbf{\sigma}, \mathbf{q}) \le f_{\max}(\mathbf{x}) + \frac{\ln(N)}{\rho} \tag{5.7}$$

Then the equivalent optimization problem to be considered with combined constraints method is:

$$(\mathbf{\sigma}_{n+1}, \mathbf{q}_{n+1}) = \mathrm{ARG} \left\{ \begin{array}{l} Min\left[\dfrac{1}{2}\left(\sigma_{n+1}^{trial} - \Sigma\right) : \mathbf{C}^{-1} : \left(\sigma_{n+1}^{trial} - \Sigma\right) + \\[2mm] \dfrac{1}{2}(\mathbf{q}_n - \mathbf{q}) : \mathbf{D}^{-1} : (\mathbf{q}_n - \mathbf{q})\right] \\[2mm] Subject\ to: \\[2mm] f(\Sigma, \mathbf{q}) = \dfrac{1}{\rho}\ln\left\{\displaystyle\sum_{\alpha=1}^{N} \exp\left[\rho\left(\dfrac{|\Sigma : \mathbf{P}^{\alpha}|}{\tau_y^{\alpha}} - 1\right)\right]\right\} \le 0 \end{array} \right\} \tag{5.8}$$

Based on the above combined constrained optimization method a new yield function for single crystals can be proposed as:

$$f(\mathbf{\sigma}, \mathbf{q}) = \frac{1}{\rho}\ln\left\{\sum_{\alpha=1}^{N} \exp\left[\frac{\rho}{m}\left(\frac{|\mathbf{\sigma} : \mathbf{P}^{\alpha}|}{\tau_y^{\alpha}} - 1\right)\right]\right\} \tag{5.9}$$

where parameter m was introduced into equation (5.9) to give more flexibility to the shape of the yield function.

Based on the normality rule, the rate of plastic deformation can be obtained by:

$$\mathbf{D}^p = \lambda \partial_{\sigma} f(\mathbf{\sigma}, \mathbf{q}) \tag{5.10}$$

or

$$D^p = \lambda \frac{\sum_{\alpha=1}^{N} \frac{\text{sgn}(\sigma : P^\alpha)}{g^\alpha} \exp\left[\frac{\rho}{m}\left(\frac{|\sigma : P^\alpha|}{g^\alpha} - 1 \right) \right] P^\alpha}{m \sum_{\beta=1}^{N} \exp\left[\frac{\rho}{m}\left(\frac{|\sigma : P^\beta|}{g^\beta} - 1 \right) \right]}$$

(5.11)

And the rate of shear on slip systems can be obtained by equation (4.38) as:

$$\dot{\gamma}^\alpha = \lambda \frac{\frac{\text{sgn}(\sigma : P^\alpha)}{g^\alpha} \exp\left[\frac{\rho}{m}\left(\frac{|\sigma : P^\alpha|}{g^\alpha} - 1 \right) \right]}{m \sum_{\beta=1}^{N} \exp\left[\frac{\rho}{m}\left(\frac{|\sigma : P^\beta|}{g^\beta} - 1 \right) \right]}$$

(5.12)

and plastic spin can be defined by

$$\Omega^p = \lambda \frac{\sum_{\alpha=1}^{N} \frac{\text{sgn}(\sigma : P^\alpha)}{g^\alpha} \exp\left[\frac{\rho}{m}\left(\frac{|\sigma : P^\alpha|}{g^\alpha} - 1 \right) \right] w^\alpha}{m \sum_{\beta=1}^{N} \exp\left[\frac{\rho}{m}\left(\frac{|\sigma : P^\beta|}{g^\beta} - 1 \right) \right]}$$

(5.13)

5.2.1. A New Model for Dislocation Velocity

Based on the proposed single crystal yield surface, a new equation for the velocity of dislocations on a slip system, which are subjected to an external force, can be presented. As mentioned before, the relationship between slip rate and the average dislocation velocity on a slip system is expressed by equation (4.18). Substituting for

$\dot{\gamma}^{\alpha}$ from equation (5.12) into equation (4.18) and assuming that

$\lambda = \phi^{\alpha}\rho^{\alpha}b^{\alpha}\tau_y^{\alpha}F\left(\tau^{\alpha},\tau_y^{\alpha},T\right)$, the average velocity of dislocations on a slip

system can be expressed by:

$$\overline{V}^{\alpha} = \frac{F(\tau^{\alpha},\tau_y^{\alpha},T)\exp\left[\dfrac{\rho}{m}\left(\dfrac{|\boldsymbol{\sigma}:\mathbf{P}^{\alpha}|}{\tau_y^{\alpha}}-1\right)\right]\mathrm{sgn}(\boldsymbol{\sigma}:\mathbf{P}^{\alpha})}{m\displaystyle\sum_{\beta=1}^{N}\exp\left[\dfrac{\rho}{m}\left(\dfrac{|\boldsymbol{\sigma}:\mathbf{P}^{\beta}|}{\tau_y^{\beta}}-1\right)\right]} \qquad (5.14)$$

As discussed before, there are several empirical models that have been developed for dislocation velocity. Unlike other models, equation (5.14) shows that stress state and strain hardening on other slip systems also affect the dislocation velocity on a particular slip system. As will be discussed later, the parameter ρ is a function of stacking fault energy (SFE) of the material. Therefore, equation (5.14) also shows that there is a relationship between the velocities of dislocations in a crystal and its SFE. To find the function F and validate the above-proposed model, several experiments will be necessary. In this research, this model was not further studied and was left as an open topic for future research.

5.2.2 Evaluation of The Effects of The Closeness Parameter ρ on The Proposed Single Crystal Yield Function

The so called closeness parameter, ρ, is an important parameters in single crystal yield function shown in equation (5.9). The proposed yield function was studied in

order to find out how the yield function shape changes with ρ. For this purpose, let us consider the yield function (5.9) for a plastic case to be:

$$f(\boldsymbol{\sigma},\mathbf{q}) = \frac{1}{\rho}\ln\left\{\sum_{\alpha=1}^{N}\exp\left[\frac{\rho}{m}\left(\frac{|\boldsymbol{\sigma}:\mathbf{P}^{\alpha}|}{\tau_y^{\alpha}}-1\right)\right]\right\} = 0 \qquad (5.15)$$

Then by manipulating equation (5.15) one can easily obtain the following relationship:

$$\sum_{\alpha=1}^{N}\exp\left[\frac{\rho}{m}\left(\frac{|\boldsymbol{\sigma}:\mathbf{P}^{\alpha}|}{\tau_y^{\alpha}}-1\right)\right] = \exp\left(\frac{\rho}{m}\right) \qquad (5.16)$$

For a plane stress condition ($\sigma_3 = 0$), and in principle stress space, equation (5.16) is:

$$\sum_{\alpha=1}^{N}\exp\left[\frac{\rho}{m}\left(\frac{|\sigma_1 P_{11}^{\alpha} + \sigma_2 P_{22}^{\alpha}|}{\tau_y^{\alpha}}-1\right)\right] = \exp\left(\frac{\rho}{m}\right) \qquad (5.17)$$

Simplifying the problem with a plane stress condition makes it easy to evaluate the effects of the yield function parameters on the behavior of the single crystal yield surface.

Figure (5.1) shows the effect of ρ on the shape of the yield surface. The yield surfaces are shown for the plane stress condition and scaled by the critical shear stress τ_0. As can be seen, by increasing the value of ρ, the shape of the yield surface shows sharp vertices. It is well known that materials with high SFE, like aluminum, show a yield surface with sharp vertices, which is related to the high mobility of the dislocations in these materials. Therefore, one can see that there is a relationship

55

between ρ and SFE of a material. For materials with higher SFE, like aluminum, higher value of ρ should be used.
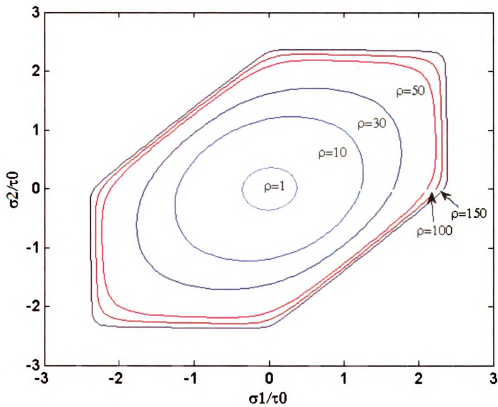
Figure 5.1 Effect of ρ on the combined constraints single crystal yield surface (crystal orientation: (100)[001])

CHAPTER 6

SOULOTION ALGORITHM FOR PROPSED CRYSTL PLASTICITY MODELS

Two different types of incremental formulation can be considered. According to an additive decompositions formulation (for hypoelastic materials) the velocity gradient is decomposed into the rate of deformation and spin tensors as $\mathbf{L} = \mathbf{D} + \mathbf{W}$ while a multiplicative decomposition of deformation is expressed as $\mathbf{L} = \dot{\mathbf{F}}\mathbf{F}^{-1}$ for hyperelastic materials. In crystal plasticity one needs to calculate the grain rotation at any increment. Therefore, crystal plasticity models are usually formulated based on hyperelastic theory. However, this type of formulation significantly increases the computation time. In this work the integrational algorithms for crystal plasticity problems are developed based on the additive decomposition formulation. Knowing that metals and alloys usually show a small elastic deformation and their constitutive models can be expressed in rate form, this type of formulation is completely valid.

Now let us rewrite the crystal plasticity problem in a strain increment $[n,\ n+1]$, based on the proposed models as:

$$\left(\sigma_{n+1}, \mathbf{q}_{n+1}\right) = ARG \begin{cases} Min\left[\chi(\Sigma, \mathbf{q})\right] \\ Subject\ to: \\ \qquad f(\Sigma, \mathbf{q}) \leq 0 \end{cases} \tag{6.1}$$

where

$$\chi(\Sigma, \mathbf{q}) = \left[\frac{1}{2} \left(\sigma_{n+1}^{trial} - \Sigma \right) : \mathbf{C}^{-1} : \left(\sigma_{n+1}^{trial} - \Sigma \right) + \right.$$

$$\left. \frac{1}{2} \left(\mathbf{q}_n - \mathbf{q} \right) : \mathbf{D}^{-1} : \left(\mathbf{q}_n - \mathbf{q} \right) \right] \tag{6.2}$$

and $f(\Sigma, \mathbf{q})$ is either one of the single crystal yield surfaces proposed in equations (3.8) and (5.9) or is one of the proposed duality functions. One should notice that if the function $f(\Sigma, \mathbf{q})$ is a single crystal yield surface then the parameter N in the equation denotes the total number of slip systems in a single crystal but if it is a duality function then N is the number of the active slip systems.

Let assume that $\mathbf{C}$ and $\mathbf{D}$ are positive definite, or in other words, the objective function χ is strictly convex in its defined domain. Although it is not proven, but let us assume that all the proposed duality functions and single crystal yield surfaces discussed in previous chapters are also convex. Now the solution to the above constrained minimization problem is to solve the following associated Lagrangian problem:

$$L(\Sigma, \mathbf{q}, \lambda) = \chi(\Sigma, \mathbf{q}) + \lambda f(\Sigma, \mathbf{q}) \tag{6.3}$$

Now the corresponding optimality condition is:

$$\begin{cases} \partial_{\Sigma} L = \dfrac{\partial L}{\partial \Sigma} = -\mathbf{C}^{-1} : \left(\sigma_{n+1}^{trial} - \sigma_{n+1} \right) + \lambda \partial_\sigma f \left(\sigma_{n+1}, \mathbf{q}_{n+1} \right) = 0 \\[2mm] \partial_{\mathbf{q}} L = \alpha_{n+1} - \alpha_n + \lambda \partial_{\mathbf{q}} f \left(\sigma_{n+1}, \mathbf{q}_{n+1} \right) = 0 \\[2mm] \partial_\lambda L = f \left(\sigma_{n+1}, \mathbf{q}_{n+1} \right) \leq 0 \\[2mm] \lambda \geq 0, \quad \lambda f \left(\sigma_{n+1}, \mathbf{q}_{n+1} \right) = 0 \end{cases} \tag{6.4}$$

These equations are equal to:

$$\varepsilon_{n+1}^{P} = \varepsilon_n^{P} + \lambda \partial_\sigma f\left(\sigma_{n+1}, \mathbf{q}_{n+1}\right),$$

$$\alpha_{n+1} = \alpha_n + \lambda \partial_q f\left(\sigma_{n+1}, \mathbf{q}_{n+1}\right),$$

$$f\left(\sigma_{n+1}, \mathbf{q}_{n+1}\right) \leq 0,$$

$$\lambda \geq 0, \tag{6.5}$$

$$\lambda f\left(\sigma_{n+1}, \mathbf{q}_{n+1}\right) = 0$$

Also let us add the following expressions to the above equations;

$$\varepsilon_{n+1} = \varepsilon_n + \nabla^s\left(\Delta \mathbf{u}\right)$$

$$\sigma_{n+1} = \mathbf{C} : \left(\varepsilon_{n+1} - \varepsilon_{n+1}^{P}\right) \tag{6.6}$$

As mentioned before, vectors α and $\mathbf{q}$ define the plastic dissipation in a material. The vector of state variables $\mathbf{q}$ for the case of isotropic hardening at constant temperature will contain a single value for the grain flow stress, $-\bar{\sigma}_g$. The vector of internal variables α will contain a single value for the grain level effective plastic strain, $\bar{\varepsilon}_g^{P}$. Then, according to the above equations

$$\Delta \bar{\varepsilon}_g^{P} = \lambda \partial_{\bar{\sigma}_g} f\left(\sigma, \bar{\sigma}_g\right) \tag{6.7}$$

The grain flow stress is a function of the critical shear stress of all slip systems in a single crystal. Therefore, equation (6.7) can be rewritten as:

$$\Delta \bar{\varepsilon}_g^{P} = \lambda \mathrm{H}(\tau_y^1, \tau_y^2, ..., \tau_y^\alpha) \tag{6.8}$$

The evolution of $\overline{\varepsilon}_g^p$ with deformation is needed for the dual mixed crystal plasticity model, which has been developed based on the Gilman's dislocation velocity model (equation (4.78)). For all other proposed crystal plasticity models, the evolution of $\overline{\varepsilon}_g^p$ with deformation is not necessary.

Equations (6.5) and (6.6) can be solved implicitly or explicitly. There are several computational techniques for solving the optimization problem (6.1) implicitly or explicitly. To increase the computational speed and efficiency, an explicit formulation is used in this work. To solve the above crystal plasticity problems explicitly, an integrational algorithm based on the cutting plane algorithm is used. According to the cutting plane algorithm procedure, at a given increment, constraints of the optimization problem are linearized iteratively to find hyper planes that cut the solution domain at any iteration and remove the part of the solution domain which dose not contain the solution to the problem. Therefore, by this manner the solution domain shrinks at every iteration until the final solution to the problem is found for the increment. Linearization of the duality function or the single crystal yield surface gives:

$$f\left(\sigma_{n+1}, \mathbf{q}_{n+1}\right) = f\left(\sigma_{n+1}^{\circ}, \mathbf{q}_{n+1}^{\circ}\right) + \partial_{\sigma} f(\sigma_{n+1}^{\circ}, \mathbf{q}_{n+1}^{\circ}) : \Delta\sigma +$$

$$\sum_{\alpha+1}^{N} \partial_{\tau_y^{\alpha}} f(\sigma_{n+1}^{\circ}, \mathbf{q}_{n+1}^{\circ}) \Delta\tau_y^{\alpha} = 0 \qquad (6.9)$$

Combining equations (2.14) and (4.38) the following relationship can be written for $\Delta\tau_y^{\alpha}$:

$$\Delta \tau_y^\alpha = \lambda \sum_{\beta=1}^{N} h^{\alpha\beta} \partial_{\tau^\beta} f \left(\overset{\circ}{\sigma}_{n+1}, \overset{\circ}{q}_{n+1} \right) \tag{6.10}$$

Also from equations (6.5) and (6.6):

$$\Delta \sigma = -\lambda \mathbf{C} : \partial_\sigma f \left(\overset{\circ}{\sigma}_{n+1}, \overset{\circ}{q}_{n+1} \right) \tag{6.11}$$

Combining equations (6.9), (6.10), and (6.11) one obtains the following expression for the incremental consistency parameter:

$$\lambda = \frac{f_o}{\dfrac{\partial f}{\partial \sigma} : \mathbf{C} : \dfrac{\partial f}{\partial \sigma} - \displaystyle\sum_{\alpha=1}^{N} \sum_{\beta=1}^{N} h^{\alpha\beta} \dfrac{\partial f}{\partial \tau^\beta} \cdot \dfrac{\partial f}{\partial \tau_y^\alpha}} \tag{6.12}$$

Where f_o is the value of the function at the beginning of the iteration. Using equations (6.5), (6.6), and (6.12) together, the crystal plasticity problem can be solved explicitly. If the orientation of a grain with respect to the co-rotational materials coordinate system is defined by matrix $\mathbf{Q}$ (defined in appendix A) then a general integration algorithm for proposed single crystal yield function crystal plasticity model can be expressed as following (For simplicity in notation, assume $\tau_y^\alpha = g^\alpha$):

1. Given the known quantities ($\hat{\sigma}_j$, g_j^α, $\Delta\hat{\varepsilon}_j$, $\mathbf{Q}_j$) for a grain (crystal) at the beginning of the increment j in the material co-rotational coordinate system, rotate the strain tensor increment and stress tensor to the crystal coordinate system using grain orientation matrix:

$$\sigma_j = \mathbf{Q}_j \hat{\sigma}_j \mathbf{Q}_j^T$$

$$\Delta \varepsilon_j = \mathbf{Q}_j \Delta \hat{\varepsilon}_j \mathbf{Q}_j^T$$

2. Initialize: $i = 0$, $\sigma_{j+1}^{(0)} = \sigma_j + \mathbf{C}^e : \Delta \varepsilon$, $g_{j+1}^{\alpha}{}^{(0)} = g_j^{\alpha}$, and $\lambda_{j+1}^{(0)} = 0$

3. Calculate $f_{j+1}^{(0)}$, using equation (16). If $f_{j+1}^{(0)} \leq 0$, go to step 9

4. Compute the increment of the plastic consistency parameter from equation (31):

$$\Delta \lambda_{j+1}^{(i)} = \frac{f_{n+1}^{(i)}}{\dfrac{\partial f_{j+1}^{(i)}}{\partial \sigma} : \mathbf{C}^e : \dfrac{\partial f_{j+1}^{(i)}}{\partial \sigma} - \sum_{\alpha=1}^{N} \sum_{\beta=1}^{N} h^{\alpha\beta} \dfrac{\partial f_{j+1}^{(i)}}{\partial \tau^{\beta}} \cdot \dfrac{\partial f_{j+1}^{(i)}}{\partial g^{\alpha}}}$$

5. Compute stresses, slip resistances, and the yield function:

$$\sigma_{j+1}^{(i+1)} = \sigma_{j+1}^{(i)} - \Delta \lambda_{j+1}^{(i)} \mathbf{C}^e : \frac{\partial f(\sigma_{j+1}^{(i)}, \ g_{j+1}^{\alpha}{}^{(i)})}{\partial \sigma}$$

$$\Delta \gamma_{j+1}^{\alpha}{}^{(i)} = \Delta \lambda_{j+1}^{(i)} \frac{\partial f(\sigma_{j+1}^{(i)}, \ g_{j+1}^{\alpha}{}^{(i)})}{\partial \tau^{\alpha}} \qquad \text{For } \alpha = 1,...N$$

$$\Delta g_{j+1}^{\alpha}{}^{(i)} = \sum_{\beta=1}^{N} h_0 \left| 1 - \frac{g_{j+1}^{\beta}{}^{(i)}}{\tau_s} \right|^a \cdot \text{sgn}\left(1 - \frac{g_{j+1}^{\beta}{}^{(i)}}{\tau_s} \right) \cdot \left[q + (1-q) \delta^{\alpha\beta} \right] \cdot \left| \Delta \gamma_{j+1}^{\beta}{}^{(i)} \right|$$

For $\alpha = 1,...N$

$$g_{j+1}^{\alpha}{}^{(i+1)} = g_{j+1}^{\alpha}{}^{(i)} + \Delta g_{j+1}^{\alpha}{}^{(i)} \qquad \text{For } \alpha = 1,...N$$

6. If $f_{j+1}^{(i+1)} \leq Tol$ go to step 8, otherwise go to step 7

7. Update the consistency parameter:

$$\lambda_{j+1}^{(i+1)} = \lambda_{j+1}^{(i)} + \Delta\lambda_{j+1}^{(i)}$$

Set $i \leftarrow i+1$. Go to 3

8. Update the grain orientation

9. Rotate the stresses back to the material co-rotational coordinate system and go to step 1 for the next grain.
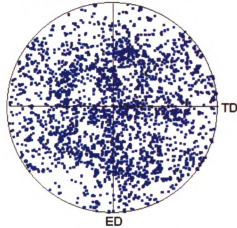
10. Homogenization

CHAPTER 7

EVALUATION OF THE PROPOSED MODELS BY MODELING OF METAL FORMING PROCESSES

To obtain the parameters of a crystal plasticity model, only a texture analysis and a uniaxial tensile test in an arbitrary direction are necessary. Therefore, crystal plasticity models are powerful tools for analyzing metal forming processes. They can be either used directly to models a metal forming process or to find the coefficients of phenomenological models.

The proposed models discussed in previous chapters were applied to the modeling of Al6061T4 polycrystalline sheet, involving uniaxial tension and tube hydroforming with different number of grains. The initial texture for the extruded Al6061-T4 tube was obtained using OIM measurement as shown in figure (7.1). Several integrational algorithms based on an explicit procedure for crystal plasticity model based on the multi yield surface proposed by Anand (1996), modified power type yield surface, dual mixed method, and the proposed combined constraint yield surface were written and implemented as VUMATs into the ABAQUS software.

(a)

(b)

Figure 7.1 a) pole figure (111) with 1005 grain orientations representing the undeformed extruded tube, and b) CODF for the undeformed Al6061-T4 aluminum extruded tube

7.1. Modeling of The Uniaxial Tension Test

Figure (7.2) shows the finite element uniaxial tensile model with 469 S4R shell element, used in these analyses. Hardening coefficients (equation (2.16)) for Al6061-T4 alloy was obtained using a multisurface crystal plasticity model proposed by Anand (1996). The components of $\mathbf{m}^{\alpha}$ and $\mathbf{s}^{\alpha}$, which are needed for equation (2.1), and the 12 slip systems used for this fcc material are shown in Table (7.1). The elastic constants for the Al6061-T4 extruded aluminum tube were determined to be; C_{11}= 108GPa, C_{12}=61GPa, and C_{44}=29GPa and the following parameters were obtained by curve fitting to the experimental uniaxial tensile data for Al6061-T4;

$$h_0 = 1285MPa\ , \tau_s = 172MPa\ , \tau_0^{\alpha} = 62MPa\ , \ and\ a = 2.0\ .$$

These parameters are kept fixed in all proposed crystal plasticity models, then other parameters of the proposed crystal plasticity models were obtained as will be explained in the following sections.
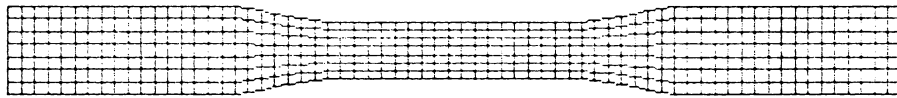

Figure 7.2. A uniaxial tensile model containing 469 S4R shell elements used in these simulations

Table 7.1. Components of $\mathbf{m}^\alpha$ and $\mathbf{s}^\alpha$ in crystal coordinate for f.c.c. materials.

α	$\mathbf{m}^\alpha$	$\mathbf{s}^\alpha$
1	$\frac{1}{\sqrt{2}} \; -\frac{1}{\sqrt{2}} \; 0$	$\frac{1}{\sqrt{3}} \; \frac{1}{\sqrt{3}} \; \frac{1}{\sqrt{3}}$
2	$-\frac{1}{\sqrt{2}} \; 0 \; \frac{1}{\sqrt{2}}$	$\frac{1}{\sqrt{3}} \; \frac{1}{\sqrt{3}} \; \frac{1}{\sqrt{3}}$
3	$0 \; \frac{1}{\sqrt{2}} \; -\frac{1}{\sqrt{2}}$	$\frac{1}{\sqrt{3}} \; \frac{1}{\sqrt{3}} \; \frac{1}{\sqrt{3}}$
4	$\frac{1}{\sqrt{2}} \; 0 \; \frac{1}{\sqrt{2}}$	$-\frac{1}{\sqrt{3}} \; \frac{1}{\sqrt{3}} \; \frac{1}{\sqrt{3}}$
5	$-\frac{1}{\sqrt{2}} \; -\frac{1}{\sqrt{2}} \; 0$	$-\frac{1}{\sqrt{3}} \; \frac{1}{\sqrt{3}} \; \frac{1}{\sqrt{3}}$
6	$0 \; \frac{1}{\sqrt{2}} \; -\frac{1}{\sqrt{2}}$	$-\frac{1}{\sqrt{3}} \; \frac{1}{\sqrt{3}} \; \frac{1}{\sqrt{3}}$
7	$-\frac{1}{\sqrt{2}} \; 0 \; \frac{1}{\sqrt{2}}$	$\frac{1}{\sqrt{3}} \; -\frac{1}{\sqrt{3}} \; \frac{1}{\sqrt{3}}$
8	$0 \; -\frac{1}{\sqrt{2}} \; -\frac{1}{\sqrt{2}}$	$\frac{1}{\sqrt{3}} \; -\frac{1}{\sqrt{3}} \; \frac{1}{\sqrt{3}}$
9	$\frac{1}{\sqrt{2}} \; \frac{1}{\sqrt{2}} \; 0$	$\frac{1}{\sqrt{3}} \; -\frac{1}{\sqrt{3}} \; \frac{1}{\sqrt{3}}$
10	$-\frac{1}{\sqrt{2}} \; \frac{1}{\sqrt{2}} \; 0$	$-\frac{1}{\sqrt{3}} \; -\frac{1}{\sqrt{3}} \; \frac{1}{\sqrt{3}}$
11	$\frac{1}{\sqrt{2}} \; 0 \; \frac{1}{\sqrt{2}}$	$-\frac{1}{\sqrt{3}} \; -\frac{1}{\sqrt{3}} \; \frac{1}{\sqrt{3}}$
12	$0 \; -\frac{1}{\sqrt{2}} \; -\frac{1}{\sqrt{2}}$	$-\frac{1}{\sqrt{3}} \; -\frac{1}{\sqrt{3}} \; \frac{1}{\sqrt{3}}$

7.1.1. Modified Power-Law Yield Surface

As discussed in equations (3.38) and (3.9), for this model there are two other parameters in the yield surface that needed to be identified. n^* can be obtained using equation (3.11) and k is obtained using curve fitting to the experimental data. For this material $n^* = 8$ and $k = 6$ were found to be the best values. Figure (7.3) shows the uniaxial results obtained by simulation using modified power-law yield surface model using 50 grains. Two different values of $k= 4$ and $k=6$ were used in this model. As can be seen, the results of the model using $k=6$ shows a good match with the experimental data. Though with using appropriate values for k one may obtain good results using the single crystal power yield surface, there are some oscillations in stresses, which may be related to the improper rotation of the grains in this model.
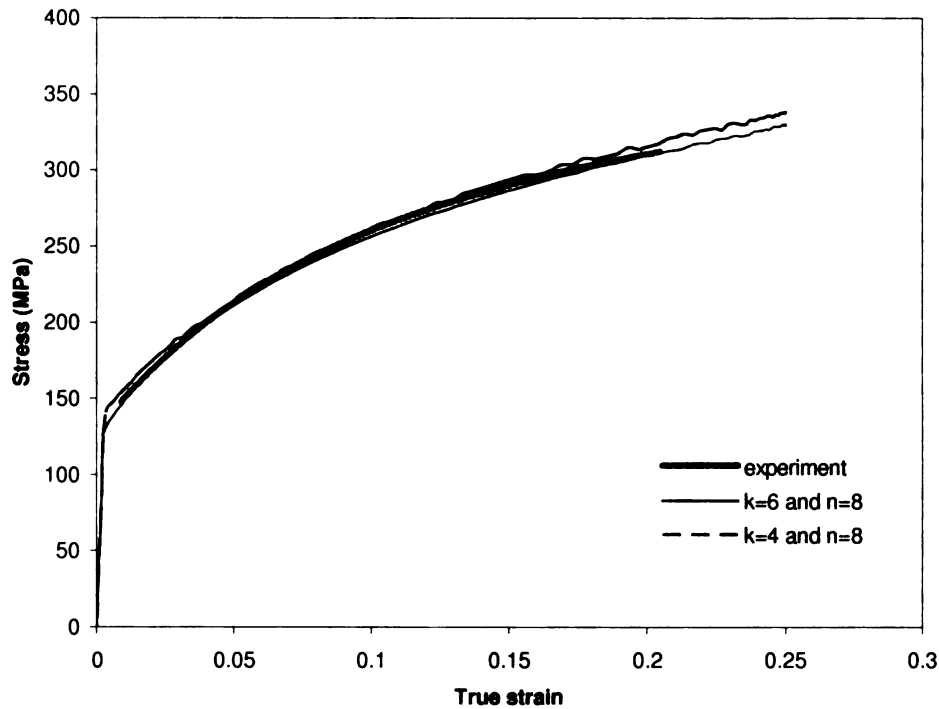

Figure 7.3. The stress – strain curves obtained by modified single crystal power yield surface

7.1.2. Dual mixed crystal plasticity models

7.1.2.1. Power Type Dual Mixed Crystal Plasticity Model

For power type dual mixed crystal plasticity model the function $h(q, N)$ in equation (4.32) should be determined. We assumed that $h(q, N) = -1$. The power of the yield function was found to be $n=2$. Then $n_2=n-1=1$ and if one assumes that $n_1=0$ then $m=1$. And this completely matches with the linear relationship that exists between dislocation velocity and the applied resolved shear stress in an aluminum single crystal. Figures (7.4) and (7.5) show the results of the power type dual mixed crystal plasticity model for uniaxial tension of Al6061-T4 alloy using 50 grains and the same hardening parameters as mentioned above. As can be seen the results of this model show a much better match with experimental data. Figure (7.6) shows the results of the simulation for the uniaxial tension using different number of grains. As can be seen using more than 10 grains yields a similar result.
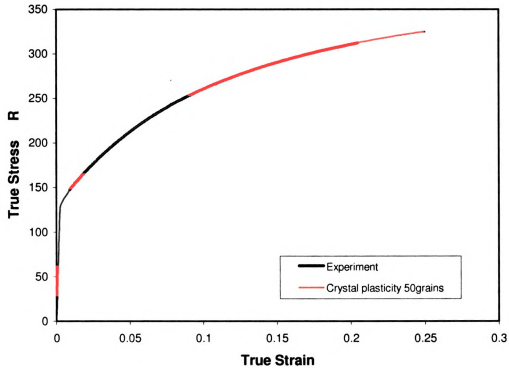
Figure 7.4. Comparison of the stress-Strain curves obtained by simulation using power type dual mixed crystal plasticity model and experiment
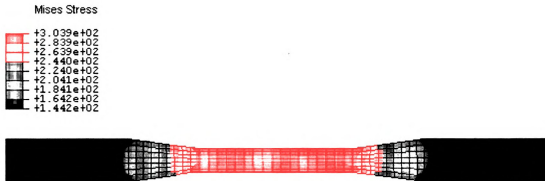

Figure 7.5. Mises stress distribution in a uniaxial tension model after 15% strain obtained by power type dual mixed crystal plasticity model
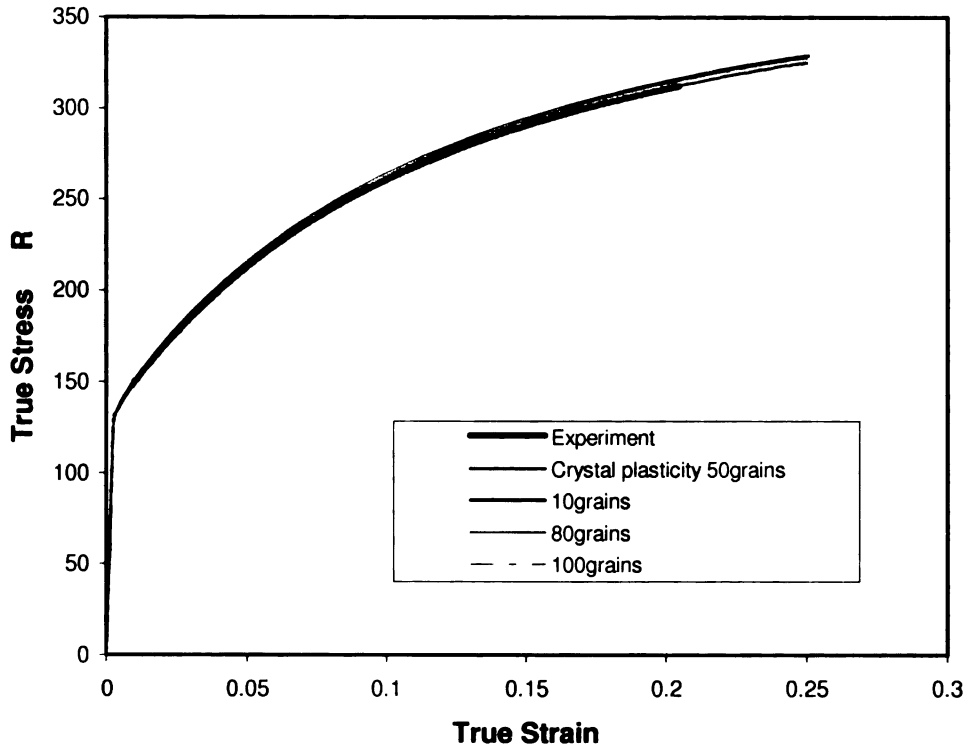
Figure 7.6. Stress-Strain curves obtained by power type dual mixed crystal plasticity model using different number of grains

7.1.2.2. Exponential Type Dual Mixed Crystal Plasticity Model

For the exponential type dual mixed crystal plasticity model the values of C^α and D^α are assumed be the same for all slip systems and equal to C and D, respectively. The results of the simulations of the uniaxial tension of Al6061-T4 alloy using 50 grains showed that if $h_1(\mathbf{q}, N) = -1$ for the model in equation (4.49) and $h_2(\mathbf{q}, N) = -\exp(D)$ for the model in equation (4.51) then $D=C$. By keeping the hardening parameters constant and the same as those obtained by Anand's model, C and D were found to be 5.0 for Al6061-T4. The uniaxial tension stress-strain curve for Al6061-T4 predicted with exponential type dual mixed crystal plasticity model

was exactly the same as the results obtained with the power type dual mixed crystal plasticity model, as shown in figure (7.4).

7.1.2.3. Dual Mixed Crystal Plasticity Models Based on Gilman's Models

For dual mixed crystal plasticity models based on Gilman's dislocation velocity models, equations (4.66) and (4.79), it was assumed that $h(N, \mathbf{q}) = \psi(N, \mathbf{q}) = -1$. Also it was assumed that for all slip systems $C_3^\alpha = C_3$, $C_4^\alpha = C_4$, and $C_5^\alpha = C_5$. Using the same hardening parameters obtained by Anand's crystal plasticity model and curve fitting the results of the simulation of the uniaxial tension to the experimental data, the parameters of the duality functions (4.66) and (4.79) were obtained to be as following:

For duality function (4.66); $n=1$, and $C_3 = 16$.

For duality function (4.79); $m=1$, $C_4 = 16$, and $C_5 = 10$.

Further investigation of the models showed that there is a relationship between the SFE of the material and parameters C_3 and C_4. In order to get results without oscillation in the stress-strain curve, C_3 and C_4 should be set to the following equation:

$$C_3 = C_4 \simeq \frac{\Gamma}{Gb} \times 10^{-3} \tag{7.1}$$

This equation is the same as equation (3.10) proposed by Gambin. Also for duality function (4.79) to avoid oscillations in stress results, the best value for C_5 can be obtained from the following equation at effective plastic strain, $\bar{\varepsilon}^P = 0.002$.

72

$$C_5 \simeq \frac{d\bar{\sigma}}{2d\bar{\varepsilon}^P} \times 10^{-2} \quad \text{(Unit of stress is MPa)} \tag{7.2}$$

where $\bar{\sigma}$ is the effective flow stress which evolves by effective plastic strain.

For evolution of $\bar{\sigma}$ in Al6061-T4 alloy the Voce equation was used:

$$\bar{\sigma} = A - B\exp(-C\bar{\varepsilon}^P) \tag{7.3}$$

The parameters of Voce equation; A, B, and C, were obtained by fitting the Voce equation to the macroscopic uniaxial tension experimental data by which the values of A=338.559 MPa, B=206.249 MPa, and C=9.822 were obtained for Al6061-T4 alloy.

7.1.2.4. Combined Constraints Crystal Plasticity Model

In addition to the strain hardening parameters, this model has two more unknown parameters m and ρ. It was assumed that m=1, then the closeness parameter ρ for Al6061-T4 alloy was found by curve fitting to the uniaxial tension experimental data, which resulted in a value of 40.75. The comparison of this model with Gambin's investigation (1997) showed that one might obtain ρ for different materials using the following expression:

$$\rho \simeq \frac{2.5\Gamma}{Gb} \times 10^{-3} \tag{7.4}$$

7.2. Modeling the Hydroforming Process of Aluminum Tubes

Hydroforming of aluminum-extruded tubes has recently been a topic of interest in automotive industry. The problem with modeling the hydroforming of an extruded tube, using a phenomenological yield function, is to find the appropriate values for the anisotropy parameters. Crystal plasticity models, which only need as input the uniaxial tension properties in the extrusion direction and the initial texture of the tube, can be used to find these anisotropy parameters for phenomenological yield functions. As part of verifying the current crystal plasticity model, tube bulging and tube hydroforming into a square die experiments were conducted and deformed shape and hoop strain distribution at the maximum pressure were measured for comparison. Table (7.2) shows the dimensions of the Al606-T4 extruded aluminum tube used in the tube hydroforming experiments. In all tube hydroforming analyses 50 grains were used in crystal plasticity models with initial orientations obtained from ODF shown in figure (7.1).

Table 7.2. Dimensions of the Al6061-T4 tube

Length (inch)	OD (inch)	Thickness (inch)
8.0	2.0	0.05

7.2.1. Modeling of The Tube Bulging Into The Round dies

Figure (7.7) shows the geometry of the die used to model the bulging of the Al6061-T4 tubes. Due to the symmetry and to decrease the simulation time, only one-quarter of the tube was considered in the modeling (figure 7.8). 174 shell elements were used

in the model as is shown in figure (7.8). Boundary and forming conditions used in the simulation were similar to the experiment where a maximum axial feed of 3mm was applied to each end of the tube while the tube was expanded with a maximum pressure of 14.18 MPa. ABAQUS symmetry boundary condition command (YSYMM) was used to apply boundary condition on the edges of tube in the symmetry directions. The friction coefficient between the die and the tube was assumed to be 0.02. During the simulation, both the internal pressure and the axial feed were linearly increased to their maximum value as a function of time. Figure (7.9) shows a bulged aluminum tube and figure (7.10) shows the results of the tube bulging simulation using the crystal plasticity proposed by Anand et al. (1996) at MIT. Figures (7.11) to (7.16) show the results of the simulation of the bulging of the aluminum tube using the proposed crystal plasticity models. As can be seen form these figures and figure (7.17), which shows the hoop strain distribution along the length of the bulged tube, all crystal plasticity models predict almost the same hoop strains with a good match with experimental data.
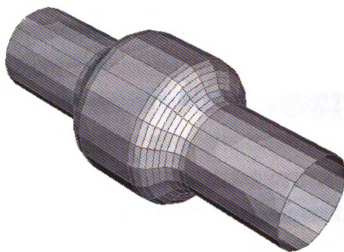
Figure 7.7. Geometry of the die used in modeling of the tube bulging
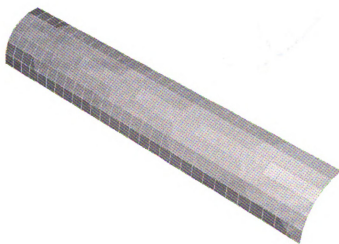
Figure 7.8. Mesh and the geometry of the one-quarter model of the tube used in modeling of the tube bulging

Figure 7.9. Bulged aluminum tube

Hoop strain

+2.023e-01
+1.857e-01
+1.691e-01
+1.525e-01
+1.360e-01
+1.194e-01
+1.028e-01
+8.622e-02
+6.964e-02
+5.307e-02
+3.649e-02
+1.991e-02
+3.337e-03
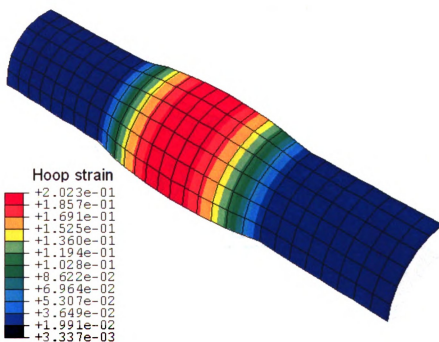
Figure 7.10. Results of the tube bulging simulation using Anand's singular value decomposition multi yield surface crystal plasticity model

Figure 7.11. Results of the tube bulging simulation using modified Gambin crystal plasticity model
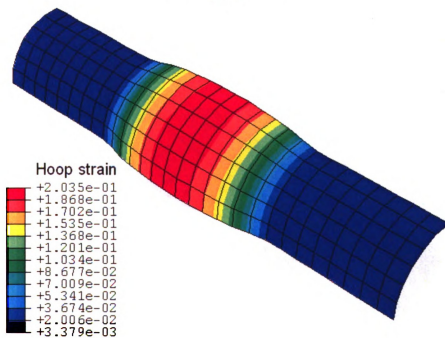
Figure 7.12. Results of the tube bulging simulation using power type dual mixed crystal plasticity model
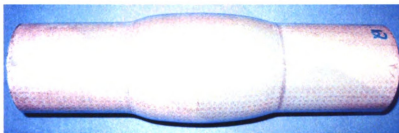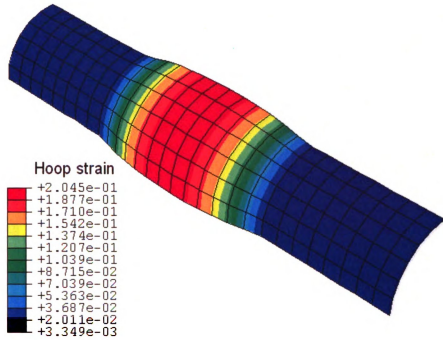
Figure 7.13. Results of the tube bulging simulation using exponential type dual mixed crystal plasticity model
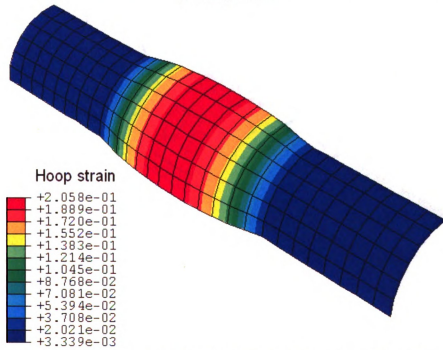
Figure 7.14. Results of the tube bulging simulation using dual mixed crystal plasticity based on Gilman model (equation 100)

Hoop strain

+2.047e-01
+1.879e-01
+1.711e-01
+1.543e-01
+1.376e-01
+1.208e-01
+1.040e-01
+8.722e-02
+7.045e-02
+5.367e-02
+3.689e-02
+2.011e-02
+3.329e-03
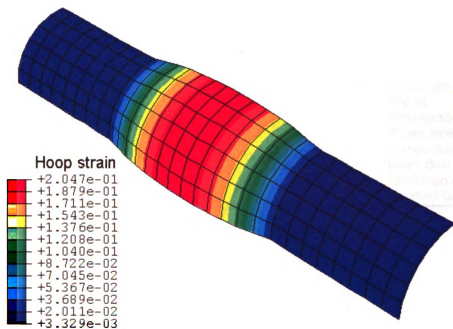
Figure 7.15. Results of the tube bulging simulation using dual mixed crystal plasticity based on Gilman model (equation 112)

Hoop strain

+2.029e-01
+1.863e-01
+1.696e-01
+1.530e-01
+1.364e-01
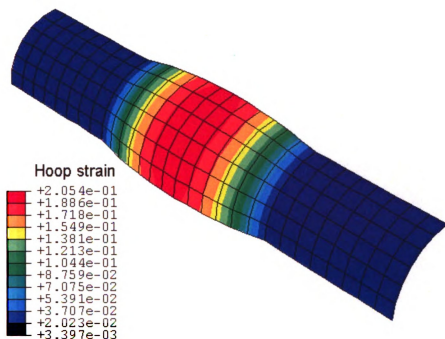+1.198e-01
+1.031e-01
+8.650e-02
+6.987e-02
+5.324e-02
+3.662e-02
+1.999e-02
+3.361e-03
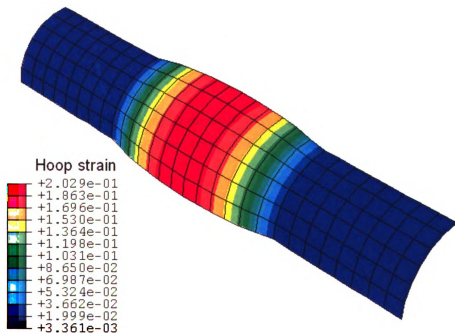
Figure 7.16. Results of the tube bulging simulation using combined constraints crystal plasticity model
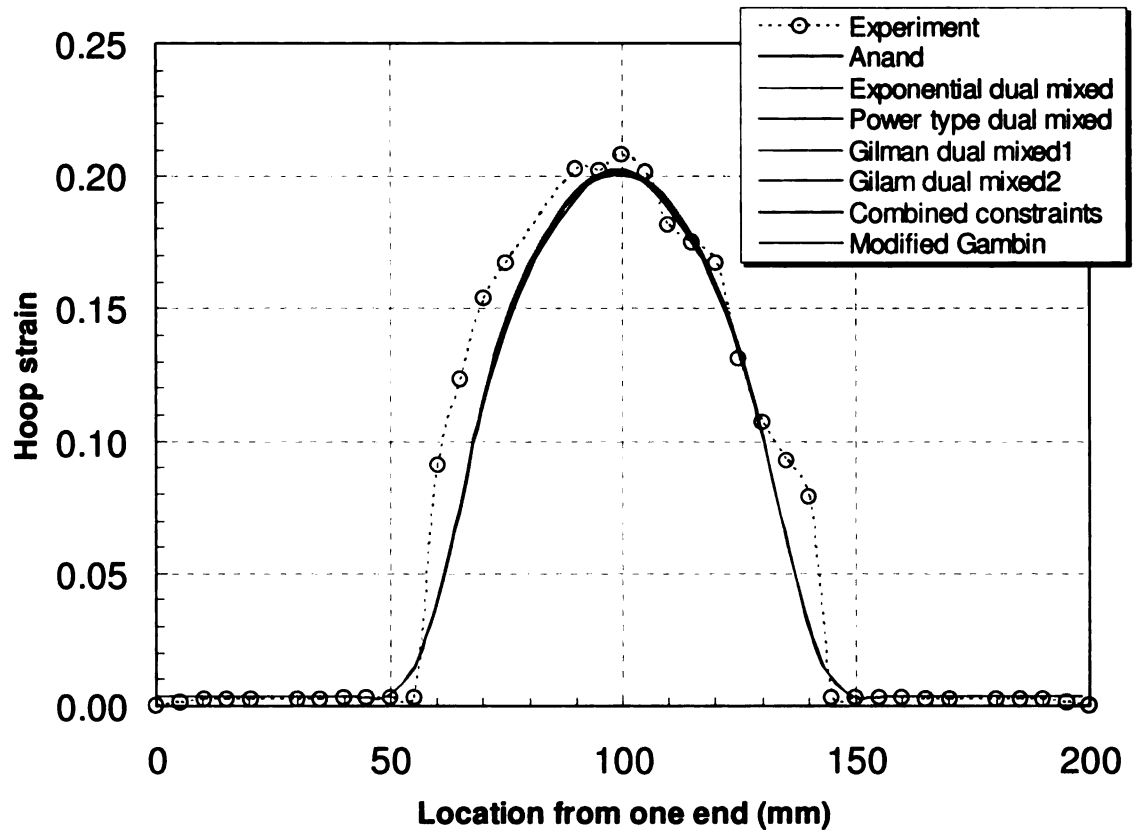
Figure 7.17. Comparison of the hoop strain distribution along the length of the tube obtained by proposed crystal plasticity models

In order to evaluate the mesh dependency of the algorithm used in the above crystal plasticity models, the simulation of the tube bulging was repeated using a very fine mesh of 2970 shell elements as shown in figure (7.18). As the computational algorithms used in all the above crystal plasticity models are based on the cutting plane algorithm, mesh dependency was tested only on one crystal plasticity model. For this purpose, the modified power type single crystal plasticity (modified

Gambin's model) was used here. Figure (7.19) shows the hoop strain distribution for this analysis. A comparison of this figure with the results shown in figure (7.10) proves the mesh independency of the computational algorithm used in the above crystal plasticity models and that with a rather coarse mesh one can obtain good results.
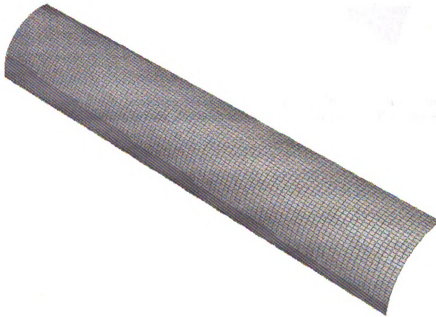
Figure 7.18. Mesh and the geometry of the one-quarter of the tube with fine mesh (2970 shell elements) used in modeling of the tube bulging

Hoop strain

+2.035e-01
+1.867e-01
+1.698e-01
+1.530e-01
+1.362e-01
+1.194e-01
+1.026e-01
+8.582e-02
+6.901e-02
+5.221e-02
+3.540e-02
+1.859e-02
+1.788e-03
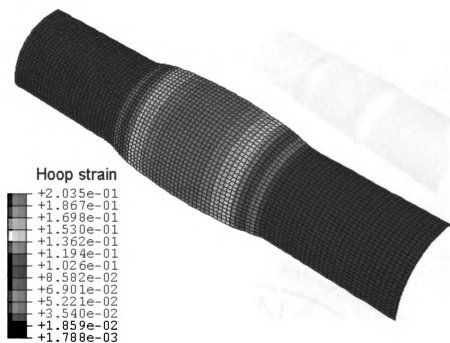
Figure 7.19. Results of the simulation of the bulging of an aluminum tube using the modified single crystal yield surface crystal plasticity model with a fine mesh (2970 shell elements)

Figure (7.20) shows the results of the crystal plasticity model for tube bulging of aluminum at different times and its comparison with experiment. As can be seen, there is a good match between the simulation and the experiment.

| Experiment | Simulation |
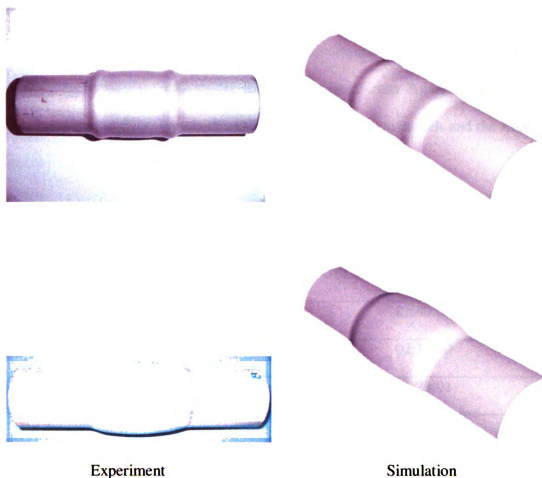
Figure 7.20. Comparison of the experiment with crystal plasticity simulation of tube bulging process of Al6061-T4 tube at different forming stages

Crystal plasticity models are usually very expensive, computationally. Therefore, it is of interest to develop novel crystal plasticity models that are more efficient or less expensive. To evaluate the computational speed of the proposed models, the total CPU times for simulating tube bulging and hydroforming of tubes into square dies were recorded and compared. Table (7.3) shows a comparison between CPU times to simulate the tube bulging process with different proposed crystal plasticity models. As can be seen from table 3, the exponential type crystal plasticity model has the best computational speed, while the SVD multi-yield surface crystal plasticity model is the

most expensive among the presented crystal plasticity models. It is also clear that the crystal plasticity models developed based on single crystal yield surface (i.e. modified Gambin and combined constraints model), are faster than Anand's model. Dual mixed models are faster than both single crystal yield surface models and the Anand's model.

Table 7.3. CPU times for the simulation of tube bulging process using different crystal plasticity models

Crystal plasticity model	CPUtime (hour/minute/second)
SDV multi-yield surface (Anand's model)	02:49:09
Modified Gambin model	02:19:00
Combined constraints model	01:29:01
Power type dual mixed model	00:52:43
Exponential type dual mixed model	00:38:46
Gilman based dual mixed model	00:44:37

One may draw an interesting conclusion by comparing the power type crystal plasticity models to exponential type crystal plasticity models. For example, the Modified Gambin model (equation 3.8) which is based on a power type yield surface for a single crystal, is more expensive than combined constraints model (equation 5.9) which is based on an exponential type yield surface for a single crystal. The power type dual mixed model is also more expensive compared to exponential type dual mixed model. Therefore, constitutive or mathematical models expressed in an exponential form are computationally faster than power type ones.

7.2.2. Modeling The Hydroforming of An Aluminum Tube Into A Square Die

To evaluate the accuracy of the model in predicting the deformation of the tube under complex strain paths, the proposed crystal plasticity models were used in the hydroforming simulation of the extruded aluminum tube into a square die. For this purpose, one quarter of the extruded tube (see Table 7.2) was modeled using 2970 shell elements (S4R). The boundary conditions used in the simulation were similar to those used in the tube bulging experiment where a maximum internal pressure of 22.34 MPa was gradually applied to expand the tube into the square die, while its ends were fixed. Figure (7.21) shows the geometry of one-half of the square die and figure (7.22) shows the mesh and the geometry of one-quarter of the initial tube used in these simulations.
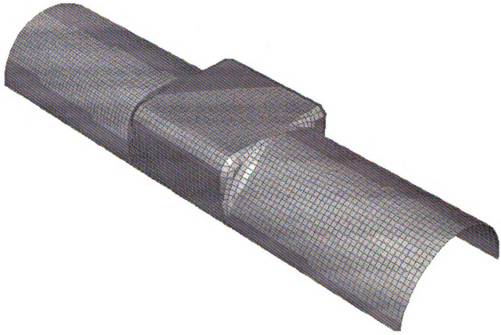
Figure 7.21. The geometry of one-half of the square die used in the hydroforming simulation of aluminum tubes
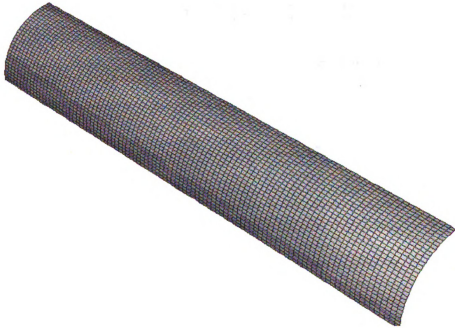
Figure 7.22. The finite element mesh used in the hydroforming simulation of one-quarter of the aluminum tube

Figure (7.23) shows the corner area of the actual hydroformed tube at the maximum pressure of 22.34 MPa. Figure (7.24) shows the failure location in the hydroformed tube once pressure was increased beyond 22.34 MPa. Figures (7.25) to (7.30) show the contour of the hoop strain predicted by different proposed crystal plasticity models. By comparing figures (7.24) and (7.25) to (7.30), it can be concluded that the crystal plasticity model has correctly predicted the location of strain localization and potential site for fracture.
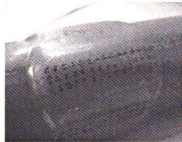
Figure 7.23. The aluminum tube hydroformed into a square die
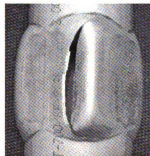
Figure 7.24. Failure location in the hydroformed aluminum tube

Figure 7.25. Hoop strain distribution in the hydroformed aluminum tube predicted by modified Gambin crystal plasticity model

Figure 7.26. Hoop strain distribution predicted by SVD multi surface (Anand's) crystal plasticity

model

```
+1.188e-01
+1.112e-01
+1.036e-01
+9.596e-02
+8.836e-02
+8.076e-02
+7.316e-02
+6.556e-02
+5.796e-02
+5.036e-02
+4.276e-02
+3.516e-02
+2.756e-02
+1.996e-02
+1.236e-02
+4.758e-03
-2.842e-03
```

Figure 7.27. Hoop strain distribution in the hydroformed aluminum tube predicted by combined constraints crystal plasticity model


```
+1.193e-01
+1.117e-01
+1.040e-01
+9.641e-02
+8.878e-02
+8.115e-02
+7.351e-02
+6.588e-02
+5.825e-02
+5.062e-02
+4.299e-02
+3.536e-02
+2.773e-02
+2.009e-02
+1.246e-02
+4.831e-03
-2.800e-03
```
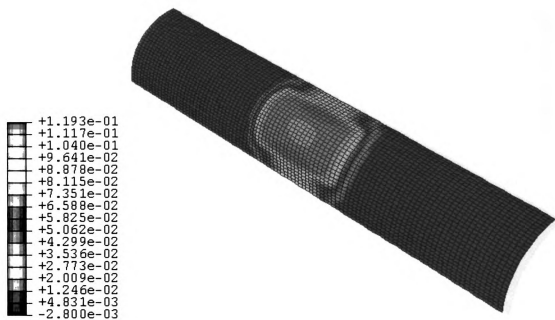
Figure 7.28. Hoop strain distribution in the hydroformed aluminum tube predicted by power type dual mixed crystal plasticity model

Figure 7.29. Hoop strain distribution in the hydroformed aluminum tube predicted by exponential type dual mixed crystal plasticity model
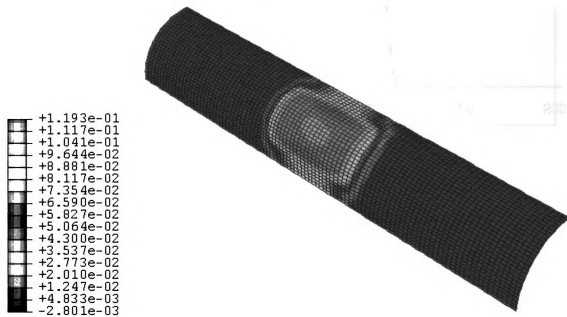
Figure 7.30. Hoop strain distribution in hydroformed aluminum tube predicted by Gilman based dual mixed crystal plasticity model

Experimentally measuring the hoop strain in the corner area of the tube, shown in figure (7.23), was very difficult and as shown in figure (7.31) there were some oscillations in the measured hoop strains. However, on the average, the simulated results obtained from the crystal plasticity models agreed very well with the experimental data.
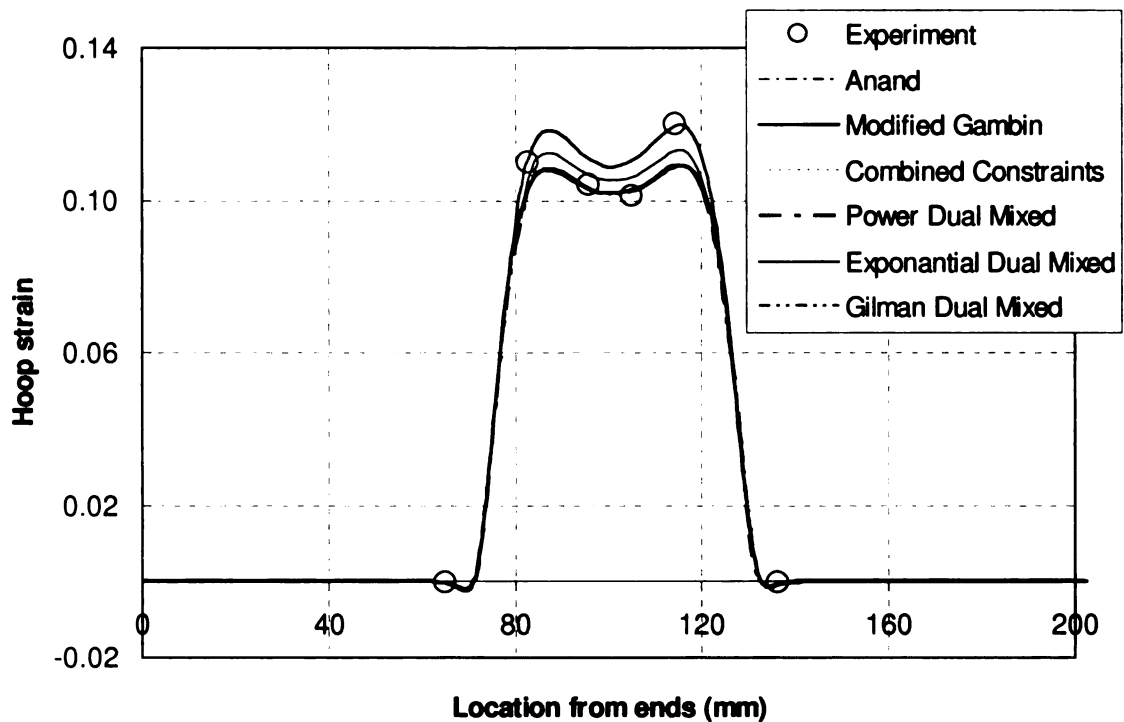
Figure 7.31. Experimental and numerically predicted hoop strain distribution along the length of the hydroformed tube

Table (7.4) shows a comparison of the CPU times for above tube hydroforming simulations by different crystal plasticity models.

Table 7.4. CPU times for simulation of hydroforming of tube into square die using different crystal plasticity models

Crystal plasticity model	CPUtime (hour/minute/second)
SDV multi-yield surface (Anand's model)	25:40:05
Modified Gambin model	23:31:03
Combined constraints model	19:13:02
Power type dual mixed model	13:12:32
Exponential type dual mixed model	10:03:46
Gilman based dual mixed model	11:17:41

CHAPTER 8

3D MODELING OF THE SURFACE PRPERTIES OF CRYSTALLINE MATERIALS

Electron work function (EWF) and phonon emission are two important surface properties in materials. EWF usually is defined as the minimum energy required to remove an electron from the interior of a solid to a position just outside the solid [Ashcroft and Mermin, (1976)]. EWF is one of the fundamental characteristics of a metallic solid and can be used in the studies of tribological phenomena including; wear, friction, oxidation, deformation, phase transformations, changes in surface composition, and surface adhesion, etc. See DeVechio et al. (1998), Zharin et al. (1998), Bhushan et al. (2000), Zharin (2001).

Phonon emission is another important parameter, which is usually considered as a measure of the thermal properties of a surface. Surface condition has a significant effect on these two parameters. Several investigations have shown that surface roughness, imperfections, dislocation density, grain boundary, plastic deformation, and crystal orientation have significant effects on both EWF and phonon emission of a surface [Van Sciever et al. (1996), Li et al. (2002), Romanowski et al. (1988), Haas et al. (1977), Stranger et al. (1973), Li et al. (2004)].

Li et al. (2004) reported that plastic deformation always decreases the EWF of crystalline materials irrespectively of whether it is tensile or compressive. Levitin et al. (1994) indicated that the EWF variation is probably related to the formation of new surfaces caused by deformation. In the following works, Levitin et al. (2001) suggested that the change in the EWF caused by plastic deformation might be also

related to dislocation behavior. More recently, Li et al. (2002) proposed a simple model to show how dislocations impact EWF. In a different work, Zharin et al. (2001) showed that the variation of EWF depended on the roughness of deformed surfaces. It was also proposed that the change in the Fermi level or the band gap during the plastic deformation may also affect the EWF [Mamor et al. (1995) and Rueda et al. (1999)].

Despite intense research over the past few decades, a complete understanding of mechanisms that are responsible for the EWF changes during the plastic deformation of a crystalline material has not yet been achieved. Fore example, there are no significant researches about the effect of the surface microstructure on the EWF and phonon emission of the crystalline materials. Usually experimental study of these effects is very difficult, expensive, or sometime impossible. Therefore, a computational investigation can be a good replacement for experimental studies.

To investigate the relationship between the surface texture and large area EWF and phonon emission, a multi-scale computational scheme coupled with a homogenization technique, which allows for accounting for the real surface microstructure of materials, should be used. However, this type of mathematical modeling is very expensive or impossible and also the more important drawback is that a mathematical framework relating the surface properties to the EWF and phonon emission have not yet been established. Considering above drawbacks, the current investigation is only focused on a few grains having the main components of a surface texture on a small region on the surface of the material. These types of simulations would be very powerful tools for studying the effects of the adjacent grain orientations and different

surface texture components on the surface dislocation density and surface roughness. In this work the combined constraints crystal plasticity model is used to investigate the effects of the surface texture and crystal orientation on the surface roughness and dislocation density, and therefore on EWF and phonon emission of the plastically deformed crystalline materials. In a given strain path, single crystals with the same orientation but different mechanical properties and crystal structures can have different plastic behaviors and therefore, different impacts on plasticity induced EWF and phonon emission of materials. In this investigation, however, the high purity niobium [Zamiri et al. (2006, 2007)] as an example of crystalline material to study the surface texture effects on EWF and phonon emission. Niobium has a bcc crystal structure and has 24 {110}<111> and {112}<111> type slip systems [Baars et al. (2008)]. Both EWF and phonon emission are important parameters in high purity superconducting niobium which is used in fabrication of the superconducting accelerator cavities, see Zamiri et al. (2006).

8.1. Experimental and Modeling Procedure

To find the main initial texture components, an Orientation Imaging Microscopy (OIM) was used to measure the initial through thickness texture of the high purity niobium sheet samples. The material used in this study was high purity superconducting niobium (RRR) sheets made by Tokyo Denkai Company with 2 mm thickness. The electropolishing technique used to prepare the sample surface for OIM study was 90% H_2SO_4 and 10% HF at 0°C using a tungsten electrode at a potential of 15V. This information was necessary for the modeling part of our investigation.

The combined constraints crystal plasticity model was used to investigate the effect of the surface texture on the plasticity induced surface roughness and dislocation density in high purity superconducting niobium.

A computational model, as shown in figure 8.1, was used in this work to study the behavior of different crystal orientations on surface behavior of the niobium during the plastic deformation. To study only the effects of grain orientations, it is assumed that all grains have the same geometry. The computational model represents a small region of the surface down to the mid-thickness of the niobium. The surface and the subsurface of the niobium sheet are presented by the grains with the same geometry and all other layers below the mid-thickness of the niobium sheet are assumed to be isotropic. This computational model is applied to simulate the uniaxial tension along axis 1.

8.2. Results and Discussion

Texture measurement showed different through thickness texture layers in the investigated superconducting niobium sheet. As the surface behavior is our interest in this study, we only analyzed the texture of the surface and a layer close to the surface (subsurface layer) of the niobium samples. The Orientation Distribution functions (ODFs) for the surface texture and subsurface texture of the niobium are shown in figure 8.2. The analysis of these ODFs shows that there is a strong (111)[11-2] component in the subsurface texture layer of niobium while the surface has a very strong (100)[001] component, and also (110)[1-10] and (111)[11-2] components with less intensity. Other OIM measurements from other regions of the niobium sheet

showed the same results. By using this information, in the first simulation we assumed that a small region on the
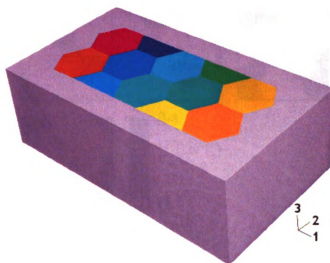
a)
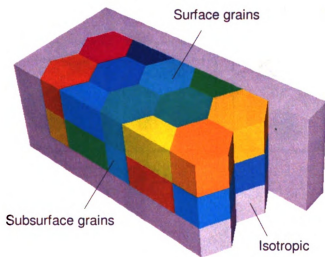
b)

Figure 8.1. The computational model that was used in these investigations; a) the whole model, b) a portion of the model showing the surface and subsurface grains
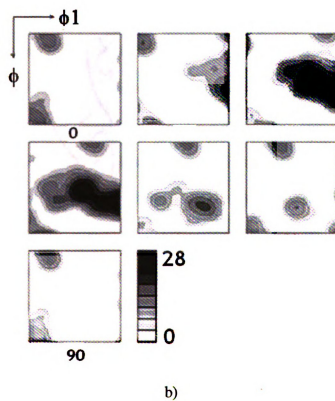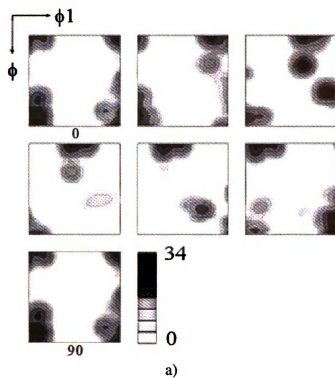
Figure 8.2. ODFs of a) surface, and b) subsurface textures of high purity niobium

surface of the niobium is made up of four grains with two of those having (001)[100] orientation and the other two having (110)[1-10] and (111)[11-2] orientations, as shown in figure 8.3. The corresponding four grains in the subsurface layer were assumed to have (111)[11-2] orientation as was measured by OIM. This type of simulation will help us to study the effects of specific orientations, and also the impact that adjacent grains have on the surface behavior during the plastic deformation.
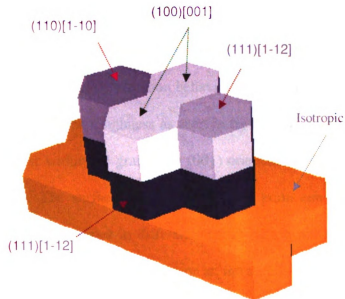
Figure 8.3. A portion of the computational model (figure1a) showing the orientation of the 4 surface and corresponding subsurface grains. All other parts of the computational model, except for these 8 grains, are considered to be isotopic

Figure 8.4 shows the results from the uniaxial tension simulation with this model along the 1 axis up to 0.4 strain. As can be seen, a surface roughness develops on the surface of the niobium after the plastic deformation. Grains with (001) orientations on the surface show a stronger tendency for through thickness and transverse deformation. (110)[1-10] component shows the least through thickness deformation among these three orientations but its transverse deformation is something between (001) and (111) components. (111)[1-12] orientation shows a more moderate deformation in all three directions. The plastic behavior of a crystal depends on the number of slip systems that become activated in the crystal during a particular strain path. The number of activated slip systems depends on the orientation of the crystal. Therefore, in a given strain path, crystals with different orientations have different plastic behavior. This different deformation behavior in different grains on the surface of niobium leads to a surface roughness as seen in figure 8.4. A small scale surface roughness is also clear within the grain with (001) orientation while it is not present in other orientations. The surface roughness within a grain can be related to the presence of different stress states in different regions of a grain and also at higher strains to the development of a microtexture or an intracrystalline misorientation due to a possibly nonuniform plastic deformation within a grain. An intracrystalline misorientation leads to different deformation behaviors in different regions, which causes a surface roughness to develop within a grain. We evaluated the amount of intracrystalline misorientation by calculating the amount of rotation of normal to the

surface of the grain, (hkl), in different regions of the surface of a grain after the plastic deformation.

a)

b)
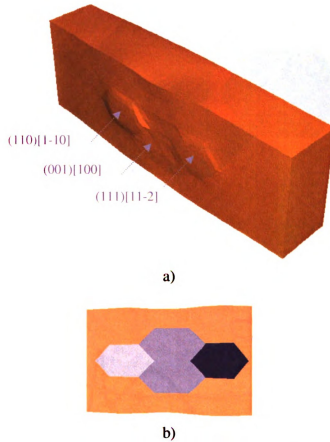
Figure 8.4. a) Surface roughness developed after plastic deformation under uniaxial tension up to 40% strain, b) the transverse plastic deformation in different grains; (111) grain (black) shows the least amount of transverse deformation while (001) grains (dark gray in the middle) show the highest

Figure 8.5 shows that the variation of intracrystalline misorientation is much higher within the grain with (001)[100] compared to the (111)[1-12] orientation. Therefore, the grain with {001} orientation shows much more inhomogeneous plastic deformation on the surface compared to the grain with {111} type orientation.

In a different simulation analysis, two grains with (111)[1-12] and (001)[100] orientations are considered to be on the surface and the corresponding grains on the subsurface have (111)[1-12] orientations (figure 8.6). The grains on the surface are
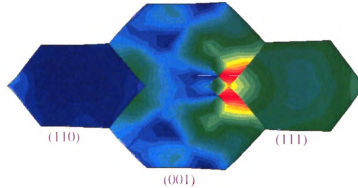
a)
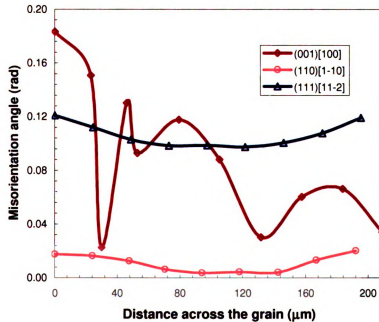
b)

Figure 8.5. The distribution of the misorientation in different surface grains, a) the contour plot (blue=0° rad and red =0.25° rad), b) the magnitude of the misorientation across the grains
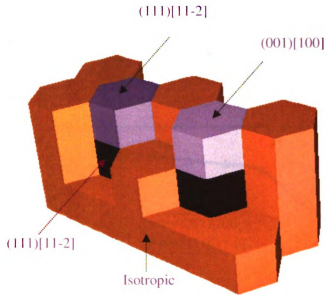
Figure 8.6. A portion of the computational model (figure 8.1a) showing the surface grains orientations and subsurface grains orientations. All other parts of the model, except for these 4 grains, are considered to be isotropic

placed a distance apart from each other in the symmetric loading positions in order to remove the effect of the adjacent grains on the deformation of the investigating grain. Figure 8.7 shows the through thickness variation of the strain from one side of the grain to the other side after the uniaxial tension up to 0.4 strain in direction 1. The through thickness strain in all regions of the grain with cube or (001) orientation is much higher than the grain with (111) orientation. Within the grain with (111) orientation, strain is minimum in the center of the grain and it increases as it approaches to the grain boundary. In other words, grains with (111) orientation have more resistance to through thickness deformation compared to the surrounding isotropic medium. The strain distribution is completely inverse in the grain with (001)

orientation in which the through thickness strain is maximum in the center and it decreases as it reaches to the grain
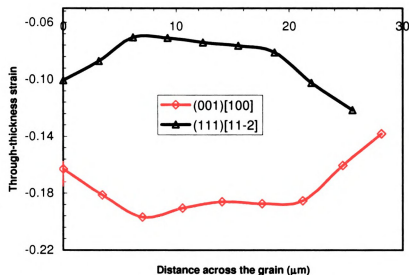
Figure 8.7. The distribution of the through-thickness strain across the grains from one side to the other side

boundaries. Based on these observations, it seems that the grain with (111) orientation tends to develop a dome shape on the surface while the grain with (001) orientation more likely develops a shape like a cavity on the surface. The effect of the different grain orientations on the surface roughness can be also investigated as discussed above.

Li et al. (2006) showed that dislocation density also has a significant impact on EWF. It is well known that the dislocation density is a function of the rate of shear strain [Dieter (1976)] and can be represented by:

$$\dot{\gamma}^{\alpha} = \phi^{\alpha} \rho^{\alpha} b^{\alpha} \overline{v}^{\alpha}$$

(8.1)

where ϕ^α is a correction factor taking into account the effect of the activation of the different independent slip systems, ρ^α is the dislocation density, b^α is Burgers vector, and $\overline{V}^\alpha$ is the average dislocation velocity on slip system α.

The rate of plastic work per unit of volume in a single crystal is expressed as:

$$\dot{w}^P = \sum_{\alpha=1}^{N} \dot{\gamma}^\alpha \cdot \tau_y^\alpha \tag{8.2}$$

The rate of critical resolved shear stress, τ_y^α, is also a function of the slip rate as:

$$\dot{\tau}_y^\alpha = \sum_{\beta=1}^{N} h^{\alpha\beta} \left| \dot{\gamma}^\beta \right| \tag{8.3}$$

Comparing equations (8.1), (8.2), and (8.3), it could be concluded that any increase in plastic work can lead to an increase in dislocation density, without considering the dynamics effects.

Replacing for $\dot{\gamma}^\alpha$ in equation (8.4) from equation (5.12), one can easily see that λ in equation (5.12) is basically the rate of the plastic work per unit of volume in a crystal. Therefore, we use the accumulated λ as a measure of plastic work in the different regions of grains to explore the effect of the crystal orientation on the dislocation density and therefore on the EWF of niobium. The same simulation procedure as explained in figure 8.3 was used again in this investigation. Figure 8.8 shows the contour of the plastic work and therefore the dislocation density from one side to the other side of the grains with different orientations on the surface of niobium. As is clear, (001) orientation shows the highest amount of the plastic work

while it is much lower in the grains with (110) and (111) orientations. Also it is clear that the plastic deformation and therefore the dislocation density are not uniform in different regions of the grains. For example, for the grain with (100) orientation the plastic deformation is at the maximum near the center of the grain while it is at its minimum level near the grain boundaries. Therefore, with plastic deformation, the EWF can vary locally from one grain to another due to the presence of different dislocation density in different grains with different orientations.
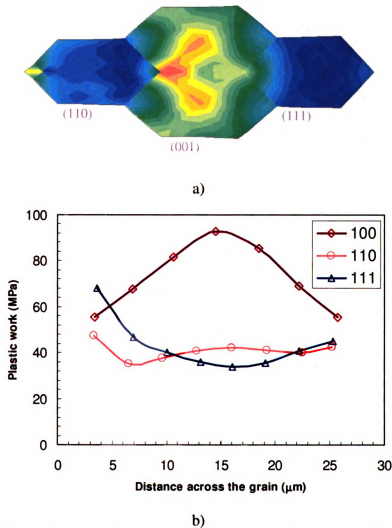

a)

b)

Figure 8.8. a) The contour plot of the plastic work inside the grains (blue=31 MPa and red=107 MPa), b) The distribution of the plastic work across grains with different orientations from one side to the other side

The EWF can be also different in different regions of a grain due to an inhomogeneous distribution of the dislocation density inside of a grain.

A random texture on the surface of the niobium leads to a surface roughness as discussed above, therefore, it decreases the electron work function of the niobium. The electron work function of the material can be a very important parameter for some applications. For example, a low electron work function leads to the electron emission or the so-called field emission in the inner surface of the niobium superconducting accelerator cavities, which decreases the performance of the cavities. According to Leblanc et al. (1974) the electron work function of pure niobium highly depends on the crystal orientation. Based on their measurements, the highest value for the electron work function belongs to {110} orientations while {001} orientations have the lowest value. As shown by the above simulations, with plastic deformation, {001} orientations develop a rough surface and also a higher dislocation density compared to the other investigated orientations. Based on these observation one can conclude that a strong surface texture with high ratio of {110}/{001} components would be desirable to have for a high value of electron work function in high purity niobium.

Phonon emission is also an important phenomenon that helps the heat transfer from the surface of a superconducting material to the coolant. Surface roughness is an important parameter that helps the phonon emission from the surface of superconducting niobium. Therefore, a more random surface texture containing some intense {001} components is desirable for phonon emission in the deformed superconducting niobium.

These types of micro-scale simulations can be easily used to design surface texture for optimal texture-dependent physical properties of the surface. There are also several other microstructural parameters that may affect the EWF and phonon emission which were not investigated in this work. For example, nonlinear strain path, grain boundary, grain geometry, and size effects are important parameters that can be further investigated.

CHAPTER 9

CONCLUSION AND FUTURE WORKS

9.1 Concluding Remarks

The critical issues in a crystal plasticity problem, especially in the rate-independent case, have been to determine active slip systems, the amount of shear on active slip systems, and the non-uniqueness due to multiplicity of slip systems. Several mathematical and computational techniques have already been developed to address these issues. However, due to persistent problems associated with calculation robustness in the current crystal plasticity models, development of more stable and efficient crystal plasticity models are still of substantial technical interest.

Three different crystal plasticity models were developed in this thesis work; Modified Gambin crystal plasticity model, dual mixed crystal plasticity models, and combined constraints crystal plasticity model.

Modified Gambin, which is a crystal plasticity model based on a power-law yield surface for single crystals, was developed to decrease the degree of non-linearity and to increase the flexibility of the previous single crystal power-law yield surfaces developed by Gambin.

A novel mathematical technique, the so called "Dual Mixed Method", was developed for solving constrained optimization problem with many constraints. This method can be used to bridge computational mathematics and other fields such as solid state physics, materials science, etc.

Up to now, several empirical models for dislocation dynamics have been developed. The dual mixed method was used to bridge the dislocation theory and the computational mechanics to develop novel temperature and microstructure sensitive crystal plasticity models, the so called "dual mixed crystal plasticity models". Their evaluation with several simulations showed that they are very CPU-efficient and fast, compared with other crystal plasticity models. Also because they have been developed using dislocation theory, they can be used to model the effect of microstructure on deformation at different temperatures. Furthermore, they can be used to model impact, room temperature creep, dynamic loading effects, micro-scale viscous deformation, deformation in semi-crystalline polymers, etc.

A crystal plasticity model is defined as a constrained optimization problem with many constraints. A single yield surface for a single crystal was found by combining these constraints using a mathematical technique. A novel crystal plasticity model, the so called "combined constraints crystal plasticity model", then was developed using this single crystal yield function. This crystal plasticity model was able to show a relationship between SFE and deformation of crystalline materials. Also this crystal plasticity model was used to develop a novel model for dislocation dynamics in crystalline materials.

All the above models were implemented into ABAQUS as user materials to simulate the uniaxial tension, and tube hydroforming of 6061-T4 aluminum alloy. Instead of hyperelasticity formulation, which is typically used in the formulation of crystal plasticity problems, an explicit updating procedure based on the consistency condition during plastic flow in the current configuration was used to improve the

execution speed and stability of the crystal plasticity models. The finite element simulation results showed that the proposed crystal plasticity models were much more efficient and faster than previous crystal plasticity models such as SVD multi-yield surface crystal plasticity and Gambin's model. The combined constraints crystal plasticity model was further used to model the effect of surface texture on surface roughness and dislocation density distribution in crystalline materials. The model was managed to successfully prediction the microtexture evolution, inhomogeneous plastic deformation, and surface roughness as already reported in literature in different surface grain of niobium as an example of its application to bcc materials.

9.2 Recommendation For Future Works

Although, all finite element simulations performed in this thesis were at room temperature, the dual mixed crystal plasticity models are temperature sensitive and can take into account the effects of temperature on plastic deformation. In contrast with other works in which only the strain hardening is considered to be temperature sensitive, the dual mixed model is a temperature sensitive crystal plasticity model. It is therefore proposed that further research be conducted where the dual mixed crystal plasticity model is applied to high temperature applications.

Further studies can be conducted where the dual mixed method can be used for the simulation of impact problems, room temperature creep, grain boundary slip transfer, micro-scale viscous deformation, Bauschinger effect, semi-crystalline polymers, etc.

The combined constraints crystal plasticity model with minor modifications will have the ability to model the cases when there is dynamic loading such as fatigue. A good research can be conducted on this topic.

Modeling based on dislocation dynamic simulation is an approach that is widely used to model the dislocation creation and dislocation interaction with second phases, inclusions, grain boundary and other dislocations. A novel dislocation dynamics model (equation 5-14) was developed in this work based on the combined constraints method. This model can relate the velocity of dislocations to the SFE and dislocation density on other slip systems. There are several unknown parameters in this model. Further researches on different crystalline materials at different temperature should be conducted to find these unknown parameters. Then this model can be used to develop a new dislocation dynamics code to model materials at smaller length scale.

The crystal plasticity models proposed above are based on Taylor type homogenization method and local based continuum theory and therefore, when length scale or size effects are of interest they cannot be used. Examples of such cases in which size effect is important are modeling of nanocrystalline materials and thin films in which grain size must be taken into account. Nanocrystalline materials are novel materials widely used in nanoelectronic devices and biotechnology. The above crystal plasticity models, especially the dual mixed crystal plasticity models, can be further improved by implementing the idea of non-local continuum theory to take into account the size effect in modeling.

Another important future research to consider would be damage in materials. Further work can be conducted to implement damage in the proposed crystal plasticity

models, especially in the dual mixed crystal plasticity models. Damage can be implemented in these crystal plasticity models by using several micro-scale damage parameters which evolve with deformation or time. These micro-scale parameters can be a function of temperature and microstructural parameters. These crystal plasticity models can then be used to obtain macro-scale damage parameters for the material.

APPENDIX A

Three Euler angles that are defined based on three different conventions, i.e. Bunge, kocks and Roe, can define the orientation of any crystal with respect to the material frame, see Bunge (1982) and Kocks, Tome and Wenk (1998). Based on the Bunge system, the orientation of a crystal can be defined by the three Euler angles $\varphi_1, \Phi, \varphi_2$ as

$$Q(\varphi_1,\Phi,\varphi_2) = \begin{bmatrix} \cos\varphi_1\cos\varphi_2 - \sin\varphi_1\sin\varphi_2\cos\Phi & \sin\varphi_1\cos\varphi_2 + \cos\varphi_1\sin\varphi_2\cos\Phi & \sin\varphi_2\sin\Phi \\ -\cos\varphi_1\sin\varphi_2 - \sin\varphi_1\cos\varphi_2\cos\Phi & -\sin\varphi_1\sin\varphi_2 + \cos\varphi_1\cos\varphi_2\cos\Phi & \cos\varphi_2\sin\Phi \\ \sin\varphi_1\sin\Phi & -\cos\varphi_1\sin\Phi & \cos\Phi \end{bmatrix}$$

(A-1)

Kocks defined the crystal orientation matrix by the three Euler angles ϕ, Ψ, Θ as

$$Q(\phi,\Psi,\Theta) = \begin{bmatrix} -\sin\Psi\sin\phi - \cos\Psi\cos\phi\cos\Theta & \cos\Psi\sin\phi - \sin\Psi\cos\phi\cos\Theta & \cos\phi\sin\Theta \\ \sin\Psi\cos\phi - \cos\Psi\sin\phi\cos\Theta & -\cos\Psi\cos\phi - \sin\Psi\sin\phi\cos\Theta & \sin\phi\sin\Theta \\ \cos\Psi\sin\Theta & \sin\Psi\sin\Theta & \cos\Theta \end{bmatrix}$$

(A-2)

And, based on the Roe definition the crystal orientation matrix is

$$Q(\psi,\phi,\theta) = \begin{bmatrix} -\sin\psi\sin\phi + \cos\psi\cos\phi\cos\theta & \cos\psi\sin\phi + \sin\psi\cos\phi\cos\theta & -\cos\phi\sin\theta \\ -\sin\psi\cos\phi - \cos\psi\sin\phi\cos\theta & \cos\psi\cos\phi - \sin\psi\sin\phi\cos\theta & \sin\phi\sin\theta \\ \cos\psi\sin\theta & \sin\psi\sin\theta & \cos\theta \end{bmatrix}$$

(A-3)

REFERENCE

ABAQUS Manual, Habbit, Karlsoon & Sorensen, INC., Providence, RI, Version 6.3

Aifantis K.E., Soer W.A., DE Hosson J. Th. M., Willis J.R., (2006) Iterface within gradient plasticity: theory and experiment, Acta Materialia, 54, 5077-5085.

Anand L., and Kothari M., (1996) A computational procedure for rate independent Crystal plasticity. J.Mech. Phys. Solids, 44 , 525-557.

Arminjon M. (1991) A regular form of the Schmid law. Application to the ambiguity problem, Textures and Microstructures, Vol 14-18, pp.1121.

Ashcroft N.W., Mermin N. D., (1976) Solid State Physics, Holt, Rinehart, and Winston, New York.

Asaro R.J. (1970), Geometric effects in the inhomogenous deformation of ductile single crystals, Acta Metall. 27, 445-453.

Asaro R.J. (1983), Micromechanics of crystals and polycrystals. Adv. Appl.Mech. 23, 1-115.

Asaro R.J. (1983), Crystal plasticity, ASME J. Appl. Mech. 50, 921-934.

Asaro R.J., Rice J.R. (1977), Strain localization in ductile single crystals, J. Mech. Phys. Solids 25, 309-338.

Asaro R.J., Needleman A. (1985) Texture development and strain hardening in rate dependent polycrystals. Acta Metallurgica, 33, 923-953.

Ashmawi W.A., Zikry M.A., (2000) Effects of grain boundaries and dislocation density evolution on large deformation modes in fcc crystalline materials, Journal of Computer Aided Materials Design, 7, 55-62.

Baars D., Jianh H., Bieler T.R., Zamiri A., Pourboghrat F., C. Compton, (2008) ICOTOM Symposium, Pittsburgh.

Bassani J.L. (1993), plastic flow of crystals. Adv. Appl. Mech. 30, 191-258.

Bassani J.L., Wu T.Y. (1991), Latent hardening in single crystals II. Analytical characterization and predictions, Proc. Royal Soc. London, A 435, 21-41.

Bhushan B., Goldade A.V., (2000) Appl. Surf. Sci. 157, 373.

Blish II R.C., Vreeland T., (1969) J. Appl. Phys., 40, 884.

Bunge H.-J. (1982) Texture analysis in materials science, Butterworths.

Busso, E., Cailletaud, G. (2005) On the selection of active slip systems in crystal plasticity. International Journal of Plasticity 21 (12), 2212–2231.

Chang YW, Asaro RJ. (1981) An experimental study of shear localization in aluminium- copper single crystals. Acta Metallurgica, 29, 241.

Chin, G. Y. and Mammel (1969), Generalization and equivalence of the minimum work (Taylor) and maximum work (BishopHill) principles for crystal plasticity. Trans. Metall. Sot. AZME 245, 1211-1214.

Chaudhuri A.R., Pate J.R., Rubin L.G., (1962), J. App. Phys., 33, 2736.

Cottrell A.H., (1958), Trans. Metall. Soc, AIME, 212, 192-203.

Cuitino AM, Ortiz M. (1992) Computational modeling of single crystals. Modeling and Simulation in Materials Science and Engineering, 1, 225-263.

Darrieulat M. and Piot D. (1996) A method of generating analytical yield surfaces of crystalline materials, Int. J. Plasticity, 12, 575-610.

DeVechio D., Bhushan B., (1998) Rev. scient. Instrum., 69, 3618.

Dieter G.E., (1976) Mechanical Metallurgy, New York (NY), McGraw-Hill.

DiMaggio F.L., Sandler I.S. (1971) Material Models for Granular Soils, Journal of Engineering Mechanics 97, 935-950.

Erickson J.S., (1962) J. App. Phys., 33, 2499.

Evers L.P., Brekelmans W.A.M., Geers M.G.D, (2004) Scale dependent crystal plasticity frame work with dislocation density grain boundary effects, International Journal of Solids and Structures, 41 (18-19), 5209-5230

Gambin W., Barlat F., (1997) Modeling of deformation texture development based on rate independent crystal plasticity, Int. J. Plasticity, 13, 75-85.

Gambin W. (1992) Refined analysis of elastic-plastic crystals, International Journal for Solids and Structures, 29, 2013.

Gambin W., (1991) Plasticity of crystals with interacting slip systems, Engineering Transaction, 39, 3-4, 303.

Gilman J.J., Johnston W.G., (1957) Dislocation and mechanical properties of crystals, Wiley, New York, p.116

Gilman J.J, (1969) Micromechanics of flow in solids, McGraw-Hill, New York, p.195

Gorman J.A., Wood D.S., and Vreeland T., J. Appl. Phys., 40 (1969) 833

Greenman W.F., Vreeland T., Jr., and Wood D.S., J. Appl. Phys., 38(1967) 3595

Gutmanas E.Y., Nadgornyi E.M., Stepanov A.V., (1963), 5, 743.

Haas G. A., Thomas R.E., (1977) J. Appl. Phys. **478**, 86.

Havner K.S., (1992), Finite plastic deformation of crystalline solids, Cambridge university press, Cambridge.

Hahn G.T., Acta Met. 10(1962) 727.

Hill R. (1966), Generalized constitutive relations for incremental deformation of metal crystals, J. Mech. Phys. Solids, 14, 95-102.

Hill R., Rice J.R., (1972), Constitutive analysis of elastic-plastic crystals at arbitrary strain, J. Mech. Phys. Solids, 20, 401-413.

Huang Y. (1991) A User-Material Subroutine Incorporating Single Crystal Plasticity in the ABAQUS Finite Element Program, Mech Report 178, Harvard University

Hutchison J.W., (1976) Elastic-plastic behavior of polycrystalline metals and composites, Proceeding of the Royal Scociety London, Series A, 319, 247-272

Johnston W.G. and Gilman J.J., J. Appl. Phys., 33 (1959) 129

Kalidindi, S. R., Bronkhorst, C. A. and Anand, L. (1992) Crystallographic texture evolution during bulk deformation processing of fee metals. J. Mech. Phys. Solids 40, 537-569.

Kim H.-K., Oh S.-I, (2003) Finite element analysis of grain-by-grain deformation by crystal plasticity with couple stress, Int. J. plasticity, 19, 1245-1270.

Kocks U.F., Tome C.N. and Wenk H.R. (1998) Texture and Anisotropy, Cambridge University Press.

Koiter W.T., (1953), Stress-Strain relations, uniqueness and variational theorems for elastic-plastic materials with a singular yield surface, Quarterly of applied mathematics 11, 350-354.

Knockaert R., Chastel Y., Massoni E. (2000) Rate-independent crystalline and polycrystalline plasticity, application to fcc materials. International Journal of Plasticity 16, 179–198.

Kreisselmeier G., and Steinhauser R., (1979), Systematic control design by optimizing a vector Performance index, proceedings of IFAC symposium on computer aided design of control systems, Zurich, Switzerland, pp. 113-117.

Kuchnicki S.N., Cuitin A.M., Radovitzky R.A. (2006) E.cient and robust constitutive integrators for single-crystal plasticity modeling. International Journal of Plasticity 22, 1988–2011

Leblanc R.P., Vanbrugghe B.C., Girouard F.E., (1974) Can. J. Phys. 52, 1589.

Lequeu, Ph., Gilormini, P., Montheillet, F., Bacroix, B. and Jonas, J.J. (1987) Yield Surfaces for Textured Polycrystals --I. Crystallographic Approach. Acta Metall., 35(5), 439.

Lequeu, Ph., Gilormini, P., Montheillet, F., Bacroix, B. and Jonas, J.J., (1987) Yield Surfaces for Textured Polycrystals--II. Analytical Approach. Acta Metall., 35(5), 1159.

Levitin V.V., Pravda M.I., Serpetzky B.A., (1994) Solid State Commun 92, 973.

Levitin V.V., Grin O.L., Yatsenko V.K., (2001) Vacuum 63, 367.

Li W., Li D.Y., (2002) Mater Sci Technol 18, 1057.

Li W., Li D.Y., (2004) Philos Mag A 84, 3717.

Li W., Cai M., Wang Y., Yu S., (2006) Scripta Mater. 54,921.

Ling X., Horstemeyer M., Potirniche, G. (2005) On the numerical implementation of 3D rate dependent single crystal plasticity formulations. International Journal for Numerical Methods in Engineering 63 (4), 548–568.

Loret, B., and J.H. Prevost, (1986) Accurate Numerical solutions for Drucker-Prager Elastic-Plastic Models, Computer Methods in Applied Mechanics and Engineering 54, 259-277.

Lublinger J. (1984) A maximum-dissipation principle in generalized plasticity, Acta Mechanica 52, 225-237

Lublinger J. (1986) Normality rules in large-deformation plasticity, Mechanics of Materials 5, 29-34

Ma A., Roters F., Raabe D., (2006) On the consideration of interface between dislocations and grain boundaries in crystal plasticity finite element modeling-theory, experiment, and simulations, Acta Materialia, 54, 2181-2194

Mamor M., Finkman E., Meyer F., (1995) Mater Res Soc Symp 356, 149.

Mandel J., (1964) Contribution theorique a l'Etude de l' ecrouissage et des lois de 1 ecoulement plastique, Proceedings of the 11th International Congress on Applied Mechanics, 502-509.

Mandel J. (1974) Thermodynamics and plasticity. Proc. Int. Symp. Foundations of Continuum Thermodynamics (ed. Delgado Domingos,J. J., Nina M. N. R. and Whitelaw J. H.), pp.283-3 Il. McMillan, London.

Mathur KK, Dawson PR. (1989) On modeling the development of crystallographic texture in bulk forming processes. Int. J. Plasticity, 5, 67-94.

McGinty, R., McDowell, D. (2006) A semi-implicit integration scheme for rate independent finite crystal plasticity. International Journal of Plasticity 22 (6), 996–1025.

Meyers M.A., (1984), Mechanical metallurgy; Principles and applications, Prentice Hall inc., New Jersey, p.304

Miehe C., Schroder J, and Schotte J (1999) Computational homogenization analysis in finite plasticity simulation of texture development in polycrystalline materials, Computer Methods in Applied Mechanics and Engineering, 171, 387-418.

Miehe C., and Schroder J (2001) A comparative study of stress update algorithms for rate-independent and rate-dependent crystal plasticity, Int. J. Numer. Meth. Engng, 50, 273-298.

Montheillet F., Gilormini P. and Jonas J.J. (1985) Relation between Axial Stresses and Texture Development during Torsion Testing: a Simplified Theory. Acta Metall., 33, 4, 705.

Naghdi, P.M.,(1960), Stress-Strain relatin in plasticity and thermoplasticity, in proceedings of the 2th symposium on naval structural mechanics, pergamon press, London.

Needleman A., Asaro R.J., Lemonds J., Peirce D., (1985). Finite element analysis of crystalline solids, Comput. Meth. Appl. Mech.Eng., 52, 689–708.

Nemat-Nasser S., Okinaka T., Ni L. (1996) A physically-based constitutive model for bcc crystals with application to polycrystal tantalum. Journal of the Mechanics and Physics of Solids 46 (6), 1009–1038.

Ney H., Labusch R., Hassen P., (1977) Acta Met., 25, 1257

Parameswaran V.R. and Weertman J., (1971) Met. Trans., 2, 1233

Parameswaran V.R., Urabe N., and Weertman J., (1972) J. Appl. Phys., 43 2982

Peirce D, Asaro R, Needleman A. (1982) An analysis of nonuniform and localized deformation in ductile single crystals. Acta Metallurgica, 30, 1087-1119.

Peirce D, Asaro R, Needleman A. (1983) Material rate dependence and localized deformation in crystalline solids. Acta Metallurgica, 31, 1951-1983.

Peirce D., Shih C.F., Needleman A., (1984), A tangent modulus method for rate ependent solids, Comput. Struct., 18, 875–887.

Pope D.P., Vreeland T., Jr., and Wood D.S., (1967) J. Appl. Phys., 38, 4011

Pourboghrat F. and Barlat F. (2002) texture evolution during hydroforming of aluminum extruded tubes, NSF-Design conference, Puetro Rico. 1958-1973.

Raphanel J.L., Ravichandran G., Leroy Y.M. (2004) Three-dimensional rate-dependent crystal plasticity based on Runge–Kutta algorithms for update and consistent linearization. International Journal of Solids and Structures 41, 5995–6021.

Resende L., Martin J.B., (1986) Formulation of Drucker-Prager cap model, Journal of Engineering Mechanics 111(7), 855-865.

Rice J.R., (1971) Inelastic constitutive relations for solids: an internal variables theory and its application to metal plasticity. J. Mech.Phys. Solids, 19, 433–455.

Rohde R.W., Pitt C.H., (1967) J. App. Phys., 38, 876

Romanowski S., (1988) Phys. Status Solidi B **145**, 467.

Rousselier, G., Leclercq, S. (2006) A simplified "polycrystalline" model for viscoplastic and damage finite element analyses. International Journal of Plasticity 22 (4), 685–712.

Rueda H., Slinkman J., Chidambarrao D., (1999) Mater Res Soc Proc 568, 245.

Sandler I.S., Rubin D., (1979) An algorithm and a modular subroutine for the cap model, International Journal of Numerical and Analytical Methods in Geomechanics 3, 173-186.

Stranger R.W., Mackie W., Swanson L. W., (1973) Surf. Sci. 34, 225.

Schadler H.W., (1964) Acta Met., 12, 861

Schmid E., Boas W., (1935), Plasticity of crystals, Chapman and Hall, London.

Simo J.C. and Hughes T.J.R. (1998) Computational Inelasticity, Interdisciplinary Applied Mathematics, Springer, New York.

Simo J.C. and Vu-Quoc L., (1986) A three dimentional finite strain rod model. Part II: Computational aspects, Comp. Methods App. Mech. Eng. 58, 79-116.

Simo J.C., Taylor R.L., (1985), Consistent tangent operators for rate independent elasto-plasticity. Comput. Meth. Appl. Mech. Eng., 48, 101–118.

Stein D.F. and Low J.R., (1960) J. App. Phys., 33,129

Stroh A.N., (1957) Adv. Phys., 6, 418

Suzuki T., Ishii T., (1968) Suppl. Trans. Jap. Inst. Met., 9, 687.

Taylor G.I., (1938) Plastic strain in metals, J. Inst. Met. 62, 307-324.

Taylor G. I. (1938b) Analysis of plastic strain in a cubic crystal. *Stephen Timoshenko 60th Anniversary Volume,* pp. 218-224. McMillan Co., New York.

Taylor G. I. and Elam, C. F. (1925) The plastic extension and fracture of aluminum single crystals. Proc. Royal Sot. London A 108,28-51.

Taylor G.I., Elam C.F., (1923), The distortion of an aluminum crystal during a tensile test, Proc. Roy. Soc. London A. 102, 643–667.

Toth L.S., Van Houtte P. and Van Bael A. (1991) Analytical Representation of Polycrystal Yield Sur-faces. in Boehler, J.P. and Khan, A.S., (eds), Anisotropy and Localization of Plastic Deformation (Proc. Plasticity '91: 3rd Int. Symp. on Plasticity and its Current Applications). Elsevier Applied Science, London, pp. 183-186.

Van Houtte P. (1987) Calculation of the Yield Locus of Textured Polycrystals using the Taylor and the Related Taylor Theories. Textures and Microstructures, 7(1), 29.

Van Sciever S.W., (1996) Helium Cryogenics, Plenum press.

Wu, T.-Y., Bassani, J. L. and Laird, C. (1991) Latent hardening in single crystals I. Theory and experiments. Proc. Royal Sot. London A 435, 1-19.

Zamiri A., Pourboghrat F., Jiang H., Bieler T.R., Barlat F., Brem J., Compton C., Grimm T.L., (2006) Mater Sci Eng A 435–436,658.

Zamiri A., Pourboghrat F., (2007) Int. J of Solids and Structures 44, 8627.

Zener c., (1948) The micromechanism of fracture, Fracturing of metals, American Society for Metals, Metals Park, Ohio

Zharin A.L, Rigney D.A., (1998) Tribol. Lett., 4, 205.

Zharin A.L., (2001) Fundamentals of Triblogy and Bridge the Gap Between the Macro and Micro/Nanoscales (Dordrecht: Kluwer Academic), p. 451.